Study on Effective Utilization of Goethite-based Nanoporous Ore

ナノ多孔質ゲーサイト基鉱石の有効利用に関する研究

by Keisuke ABE

A dissertation submitted in partial fulfillment of the
requirements for the degree of Doctor of Engineering
(Graduate school of engineering) in Hokkaido University
2017

Doctoral Committee:

Professor Tomohiro Akiyama
Professor Shigeharu Ukai
Professor Seiichi Watanabe
Associate Professor Yoshiaki Kashiwaya
Associate Professor Takahiro Nomura

Contents

Chapter 1

General Introduction

1-1. Background; problems of the ironmaking industry related to resource, environment, and energy

1-1-1. Resource problems in the ironmaking industry: high-grade ore and coal

Iron is fourth the most abundant element in the earth's crust after O, Si, and Al ones. Because of the abundance in resource, good mechanical property, and easy reduction process, iron is the most produced metal in the world. Recent worldwide economic growth causes the demand expansion of iron. The amount of steel production has been increasing year by year in the world, resulting in resource problem in the iron and steel industry.

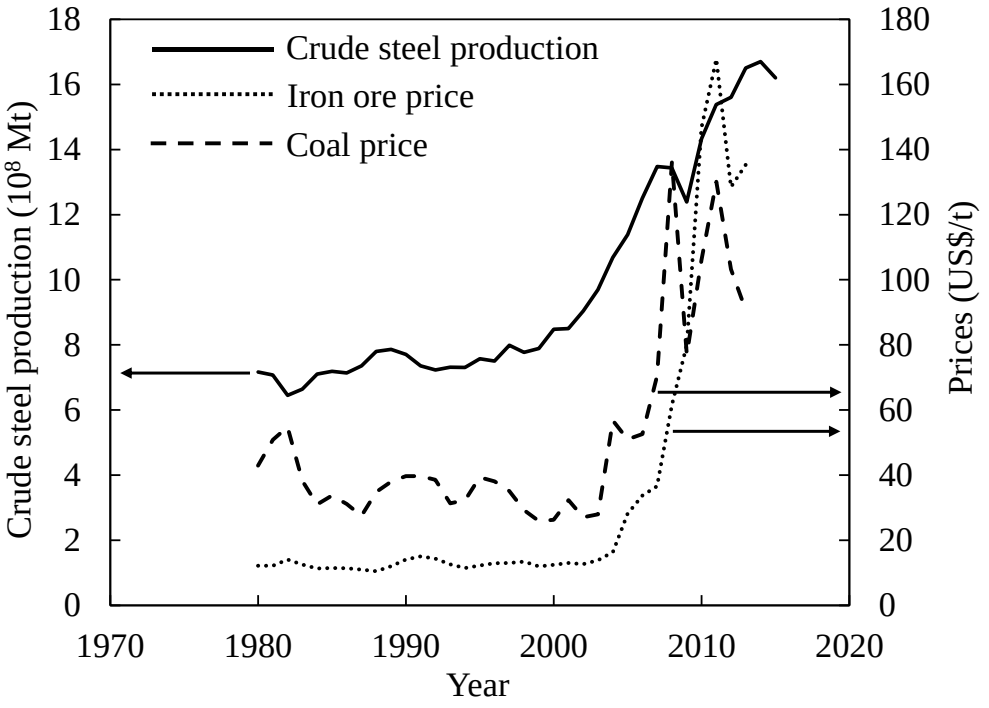

Figure 1-1. The amount of crude steel produced in the world and the prices of the high-grade iron ore and coal [1-4].

In the blast furnace ironmaking process, high-grade iron ore (sinter ore), coke (produced from strongly caking coal), and limestone are utilized to produce iron. As shown in Figure 1-1, the amount of crude steel production has been rapidly increasing worldwide for the recent 20 years. This rapid growth of the iron production causes degradation and high-price of the high-grade iron ore. Yearly transition of the prices of iron ore and coal are also shown in Figure 1-1. The iron ore in this figure was that imported by China and contained 62mass% of Fe. The coal, which was produced in Australia, contained 14mass% of ash and 1mass% of sulfur. The price of the high grade iron ore rose from 14 USD/t in 1990 to 130

USD/t in 2013. That is why, new iron ore resources which are abundant and cheap are highly needed to decrease the cost of raw materials. One of the alternate iron ore is goethite (α-FeOOH) based ore in Southeastern Asia and Oceania contains less than 60wt% of iron. The FeOOH contains combined water, which causes pulverization due to heating, makes it difficult to put the goethite ore directly into the blast furnace. That is why, the goethite ore is sent to a sintering process to remove the combined water and to obtain high-strength sintered ore.

1-1-2. Environmental problems in the ironmaking industry: large amount of CO_2 emission

The iron and steel industry has an environmental problem related to CO_2 emission. CO_2 is mainly emitted in the iron and steel industry due to combustion of fossil fuels for heat sources and production of electrical energy, reduction process of iron ores to pig iron, and final steel production. Figure 1-2 (A) shows the amount of CO_2 emission related to fuel combustion in the worldwide iron and steel industry [5-7]. The amount of CO_2 emission in the world iron and steel industry has been increasing year by year. The contribution of the CO_2 emission in the iron and steel industry to the world CO_2 emission has been also increasing; around 9% of the total CO_2 emission is contributed by this industry. Figure 1-2 (B) shows CO_2 emissions from each process in the industry. CO_2 emissions in the processes related to blast furnace account for around 50% of the total emissions.

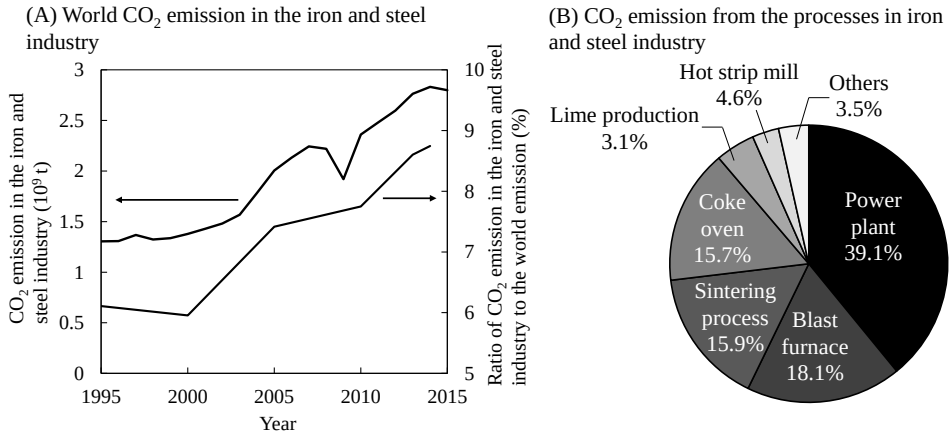

Figure 1-2 CO_2 emissions in the iron and steel industry [5-7]. (A): the amount and the ratio of CO_2 emission in the iron and steel industry and (B): CO_2 amount from each process in the iron and steel industry.

As well as blast furnace process, coke oven and sintering process which are production processes of raw materials (coke and sinter ore) for the blast furnace emits a lot of CO_2. Coke, which works as a heat source, reducing agent, and maintaining the gas flow in the blast furnace, is produced from coal in the coke oven by heating at 1200℃ for 20 h in the atmosphere without oxygen. Coke oven gas (COG), which contains H_2, CH_4, N_2, CO, and CO_2, is also produced from the coke oven. Mixture of the COG and blast furnace gas (BFG, contents: N_2, CO, and CO_2) is combusted to supply heat to the coke oven [8]. Sintering process, in which fine iron ore such as goethite ore is heat treated with fine coke and lime, produces

bigger and stronger sinter ore. The fine coke is combusted in this process to make high temperature. The combustion of COG, BFG, and fine coke causes the large amount of CO_2 emission from the coke oven and the sintering process. The purpose of these large-CO_2-emission processes is only to make raw materials optimum for the blast furnace. Ironmaking processes which do not go through the blast furnace have a possibility to reduce the amount of CO_2 emission drastically in the iron and steel industry.

1-1-3. Energetic problems in the ironmaking industry: emission of high-temperature waste heat

The iron and steel industry is one of the most energy-consuming industries. The industry used 2.3×10^{19} J in 2005 which was the second largest amount of energy usage among all industries [9]. This means that the iron and steel industry has potential to play a significant role for energy saving especially in blast furnace and coke oven processes. Because of the large amount of energy usage, the iron and steel industry emits a lot of waste heat without effective recovery. Figure 1-3 shows the examples of the amount of waste heat in the iron and steel industry [10]. The amount of unutilized waste heat based on enthalpy is higher at lower temperatures. However, the quality of the heat energy, as it is called “exergy”, is much larger at higher temperatures. The heat exergy is expressed as a function of temperature T:

$$\text{Heat exergy} = 1 - \frac{T_0}{T} \quad (1\text{-}1)$$

where T_0 is environmental temperature (298 K). It is obvious from the equation (1-1) that the heat exergy becomes larger at higher temperatures. That is why the amount of waste heat based on exergy is much larger at high temperature regardless of larger enthalpy at lower temperatures. This means high-temperature waste heat has a potential to be more effectively utilized.

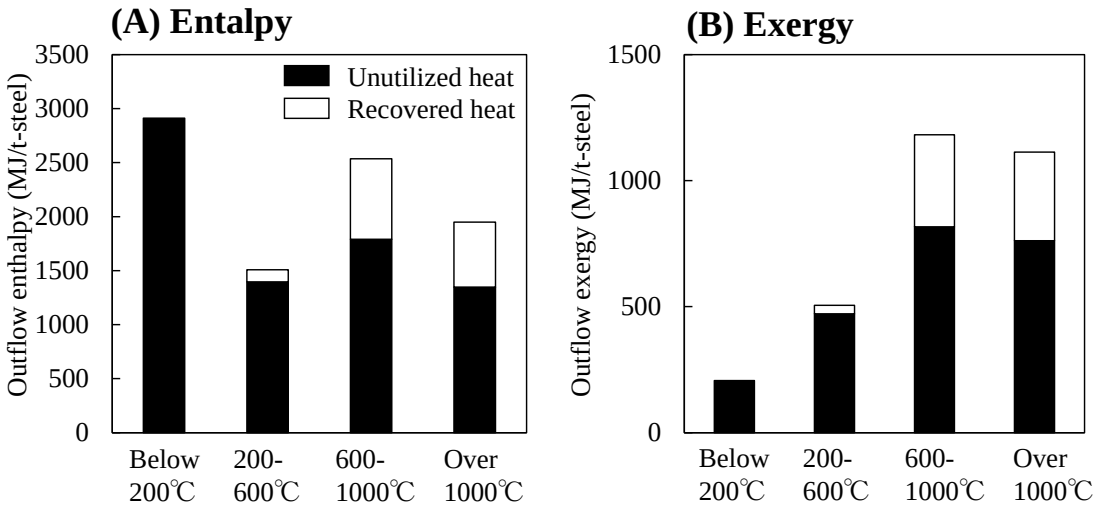

Figure 1-3 The amount of waste heat in the iron and steel industry [10].

1-2. Goethite ore

The goethite-based (α-FeOOH) iron ore is abundant in South-East Asia and Oceania but ineffectively utilized because the ore has a lot of (approximately 10mass%) combined water (CW) inside it. In the actual ironmaking process, the goethite ore is sintered with coke powder and lime at over 1400 ℃ for high strength.

It is already known that nanoporous Fe_2O_3 can be obtained by the dehydration process with mild calcination at low temperature [11-17].

$$2FeOOH\ (s) \rightarrow Fe_2O_3\ (s) + H_2O\ (g) \qquad (1\text{-}2)$$

The porous structure of the calcined FeOOH has been investigated by a lot of researchers; the pore structure changes by the calcination temperature [11-17]. At lower temperature (200-300℃) of calcination layered slit-type micropores and mesopores are generated [11, 14-17]. Dehydration reaction occurs at around 250℃ and combined water comes out from FeOOH [16], resulting in micropores (around 1 nm) in the dehydrated FeOOH. The mesopores are said to be generated by the removal of water molecules between initial crystalline of the FeOOH [16]. When the calcination temperature becomes higher (500-600℃) the pores get larger and become spherical shape [11, 14]. Calcination temperature of over 800℃ destroyes the pore structure of the FeOOH [17].

The FeOOH has an interesting property to become nanoporous material as

mentioned above, however, the goethite ore in the actual process is treated at high temperature (over 1400℃) only to satisfy the demand of the blast furnace. At the high temperature, the nanopores in the goethite ore are completely destroyed.

1-3. Utilization of Ni-containing goethite-based ore as a catalyst

1-3-1. Ni-containing goethite ore in the laterite soil

Ni is widely utilized in a lot of products such as catalysts and stainless steel. The smelting of Ni is taken place from two types of Ni ores; oxide ore and sulfide ore. Reserve estimation says that Ni oxide ore accounts for around 72% of the total ores. From the view point of Ni resource, oxide ore is much more abundant in the earth, however, sulfide ore is mainly utilized for Ni production; 58% of the Ni in the world is made from the sulfide ore [18]. That is because it is possible only for sulfide ores to condensate Ni component via flotation separation [19]. The Ni oxide ores are not used often for the production of Ni. That is why, they have potential to be used in another methods. Ni oxide ores are mainly existed in laterite soil in the south-eastern Asia and Oceania areas. Figure 1-4 shows the schematic image of the laterite soil. In the laterite soil, there are mainly three types of zone; the goethite (limonite) zone, the transition zone, and the saprolite zone [20].

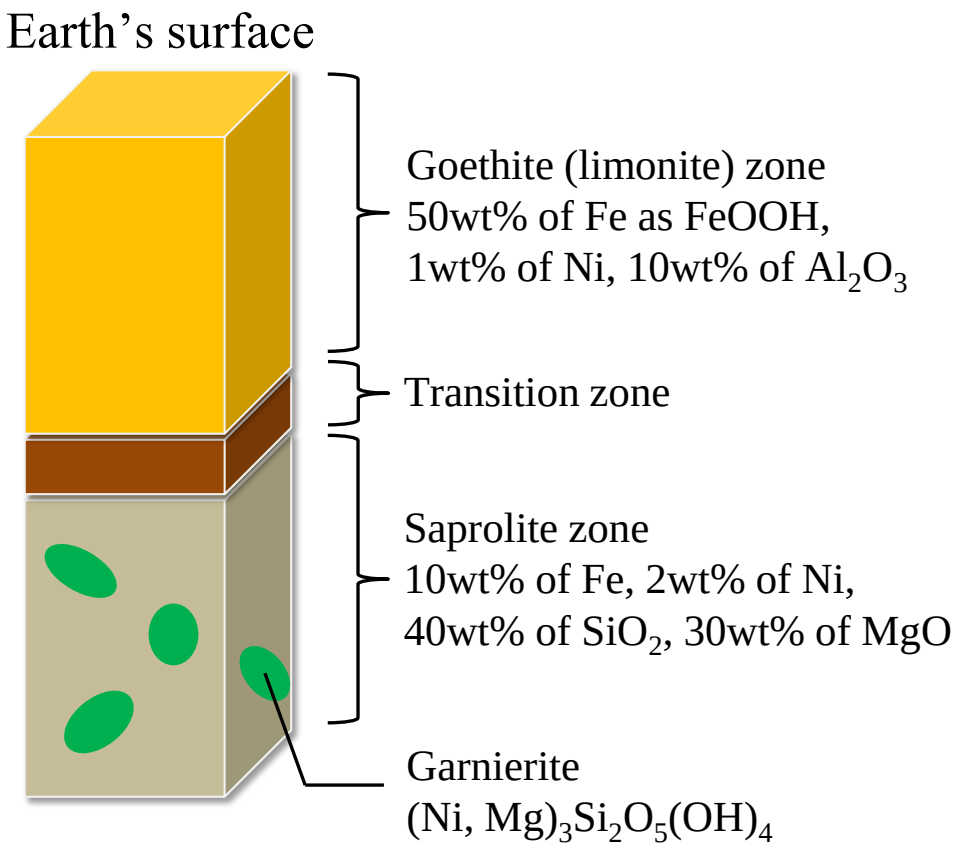

Figure 1-4 Schematic image of the laterite soil [20].

The goethite zone is located near the surface of the earth. It contains around 50wt% of Fe as a form of FeOOH and 1wt% of Ni. The FeOOH becomes nanoporous via the dehydration equation (1-2) as was mentioned above. The obtained nanoporous goethite ore has a potential to be utilized as a catalyst because it naturally contains Ni which is active catalyst in a lot of chemical reactions.

1-3-2. Goetihte ore utilization as a catalyst

The Ni-containing (around 1wt%) goethite ore which can be nanoporous after mild calcination has a potential as a catalyst for chemical reactions. A lot of studies have been conducted for the goethite ore as the catalyst of a chemical reaction. Followings are the examples of goethite ore utilization as a catalyst in some chemical reactions.

In 1979, Kiyomiya et al. investigated the reduction reaction of nitrogen monoxide with ammonia, oxygen, sulfur dioxide, and steam on the pellet which was prepared from natural Ni-containing goethite ore (from Philippine) [21]. The pellet became porous (49-90 m^2/g) as a result of mild pre-calcination before the catalytic use. The ore was durable for the reaction at least 100 h at 350℃.

Cubeiro et al. focused on Fischer-Tropsch (FT) reaction; Synthesis of carbon hydride from hydrogen and carbon monoxide [22]:

$$(2n+1)H_2 + nCO \rightarrow C_nH_{2n+2} + nH_2O \qquad (1\text{-}3)$$

They prepared ore catalyst promoted by manganese nitrate and potassium carbonate. During catalytic tests for FT reaction, the iron in the ore changed to magnetite and carbide and the carbide successfully worked as a catalyst for formation of alkenes.

Tsubouchi et al. decomposed ammonia on a pre-reduced goethite ore catalyst [23]. They reduced the ore by hydrogen at 500℃ and got metallic iron phase. The pre-reduced ore was used as a catalyst at 300-500℃ and almost of all the input

ammonia was successfully decomposed to nitrogen at 500℃. The obtained ore became nitride after the catalytic utilization.

1-3-3. Dry reforming reaction

The dry reforming reaction is attractive hydrogenation reaction from carbon dioxide and hydrocarbon.

$$C_mH_n + mCO_2 \rightarrow (n/2)H_2 + 2mCO \quad (1\text{-}4)$$

When methane is used as hydrocarbon, the reaction becomes most simple,

$$CH_4 + CO_2 \rightarrow 2H_2 + 2CO \ (\Delta H = 247 \text{ kJ/mol}, \Delta G = 0 \text{ at } 643℃) \quad (1\text{-}5)$$

where ΔH and ΔG mean the standard enthalpy change and the free Gibbs energy change of a reaction, respectively. This reaction is an endothermic one and occurs at high temperature. Akiyama et al. revealed that endothermic chemical reactions are appropriate for the recovery of high-temperature waste heat in the iron and steel industry from the viewpoint of exergy [24]. In addition to attractive method for effective heat recovery, the dry reforming reaction contributes to reduction of CO_2 emission and hydrogen production. The dry reforming reaction is known as a catalytic reaction; noble metal-based catalysts, such as Pt, show very high catalytic activity in this reaction [25]. However, the noble metals are so expensive, that is

why, comparatively cheaper Ni-based catalysts have been mainly investigated for this reaction [26].

1-3-4. Ni-containing goethite ore as a catalyst for the dry reforming of methane

As is mentioned above, the dry reforming reaction can be utilized for hydrogen production with CO_2 elimination and high-temperature waste heat recovery in the steel and ironmaking industry. Ni-containing goethite ore has more benefits as a catalyst than the conventional Ni-based catalysts.

The goethite ore has potentials to be used as a catalyst in the dry reforming of methane because it becomes nanoporous after mild calcination and contains Ni components which show high catalytic performance. Moreover, ore-based catalyst is much cheaper and produced via much more simple processes than the conventional Ni-based catalysts. Figure 1-5 shows comparison of production processes between conventional Ni/Al_2O_3 catalyst and the goethite ore catalyst. Conventional Ni/Al_2O_3 catalyst is produced from Ni nitrate ($Ni(NO_3)_2 \cdot 6H_2O$) and support Al_2O_3. Ni nitrate is produced by nitric acid treatment of metallic Ni [27]. Ni sulfide ore is firstly pulverized and beneficiated, then roasted in an oxygen atmosphere to remove iron component [28]. The obtained matte, mixture of Ni and Cu sulfide, is leached by $CuCl_2$ to give Ni solution [28]. After that, metallic Ni is obtained via electrowinning process [28]. $Al(OH)_3$ is generally used for the synthesis of Al_2O_3 [29]. $Al(OH)_3$ is synthesized via bayer method at around 250℃ from bauxite ore and NaOH and the obtained $Al(OH)_3$ is heat treated to generate

support Al_2O_3 [30]. The Al_2O_3 support is put into the Ni nitrate aqueous solution and Ni/Al_2O_3 catalyst is obtained after drying, calcination, and activation. On the other hand, the goethite ore catalyst can be prepared via very simple processes; pulverization, mild caicination for removal of combined water, and activation.

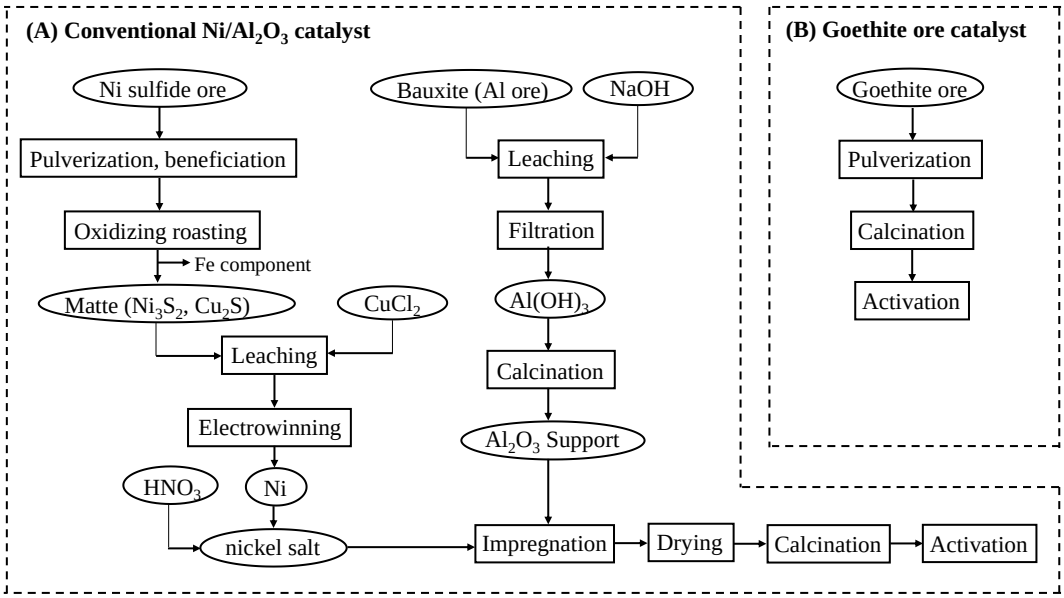

Figure 1-5 Comparison of catalyst production processes between (A): conventional catalyst and (B): goethite ore catalyst. Ni supported Al_2O_3 was chosen as conventional catalyst.

Carbon deposition on the conventional Ni-based catalyst during usage for the dry reforming reaction causes catalytic deactivation. The Ni-based catalysts are less resistant to the carbon deactivation than the noble-metal-based catalysts [31]. The

goethite ore catalysts, on the other hand, the can be recycled after carbon deactivation. The main component of the goethite ore catalyst is iron oxide; the deposited carbon can be worked as reductant of the iron oxide.

1-4. Carbon infiltrated goethite ore

1-4-1. Composites of iron ore and carbon-based materials

Blast furnace ironmaking, in which high-grade hematite ore or sinter ore, coke, and lime as raw materials, is the most common method to make metallic iron in the world.

However, almost half of the CO_2 emissions in the iron and steel industry come from the blast furnace ironmaking processes including preparation processes of the raw materials. To utilize a method without coke oven and sintering processes the amounts of CO_2 emission and energy consumption in the iron and steel industry should be decreased. A lot of attempts have been tried to develop direct ironmaking method using carbon infiltrated iron ore. Direct ironmaking method utilizes composite of iron ore and carbon material (carbon infiltrated iron ore) has been studied for coke-free ironmaking to reduce the CO_2 emissions in the iron and steel industry. Figure 1-6 shows the relationship between contact distance and reaction rate in composites of iron ore and carbon material. High reactivity between iron oxides and reducing agent is important for the reduction of the composite; Close contact of the ore and carbon make reduction faster [32]. Carbon vapor infiltration (CVI) method is attractive to make carbon-infiltrated goethite ore in which goethite ore and carbon have nanometer-scale contact.

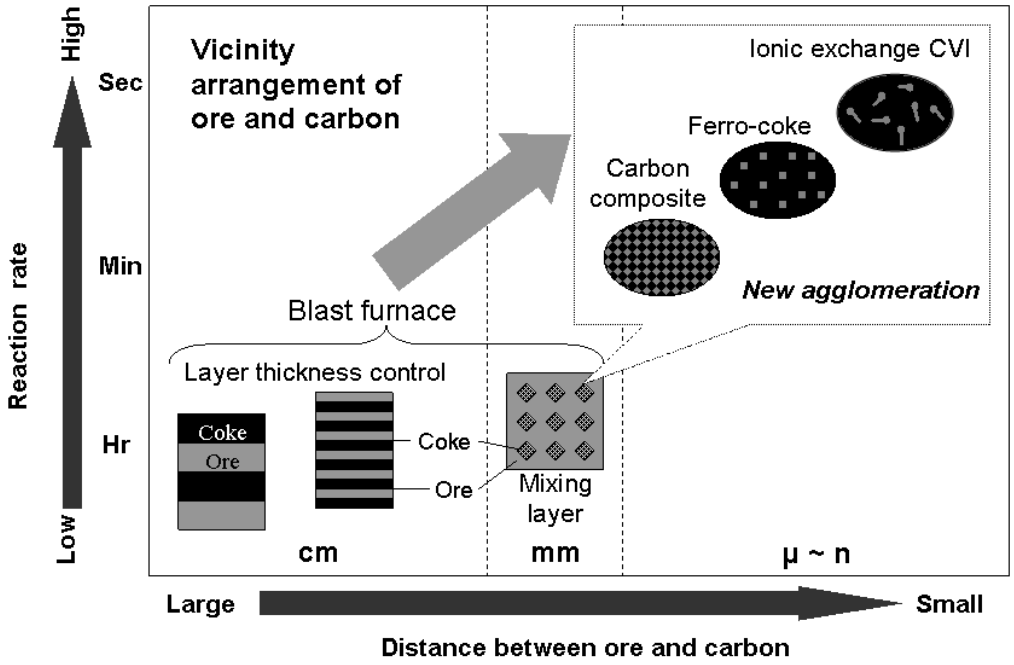

Figure 1-6 Relationship beteen reaction rate and arrangement of iron ore and carbon [33].

1-4-2. Carbon vapor infiltration methods to produce carbon infiltrated goethite ore

Carbon vapor infiltration (CVI) method have been studied to produce carbon infiltrated goethite ore (CVI ore) [34-43]. In the CVI process, carbonaceous materials containing heavy hydrocarbon such as coal and biomass are thermally decomposed to make tar vapor. Then the vapor infiltrates into the nanopores of goethite ore and decomposes into carbon, gases, and light tar components. In 2009, Hata et al. succeeded to produce CVI ore containing 1.1—4.0mass% of carbon using biomass as a carbon source [34]. Then, the obtained ore was partially reduced

to metallic iron at 900℃ [34].

Cahyono et al. then tried to utilize coal as a carbon source in the CVI process. They also observed the effects of carbon source and CVI temperature [35-40]. They used three kinds of carbon sources; high grade (bituminous) coal, low grade (lignite) coal, and biomass (palm kernel shell). They revealed coals released larger amount of tar vapor than biomass. The large amount of tar caused larger amount of deposited carbon in the CVI ore. The optimum CVI temperature was 600℃. Below 500℃, the rate of tar decomposition on the goethite ore was very slow. On the other hand, above 700℃, the rate of tar decomposition was fast, however, carbon gasification occurred and the amount of deposited carbon decreased. The highest carbon amount in the CVI ore was obtained at 600℃, the optimum temperature.

Distribution and morphology of the deposited carbon in CVI ore were also reported [41]. The deposited carbon was located only near the surface of the goethite ore and almost no carbon was detected in the center part. This is because the rate of carbon deposition might be much higher than that of infiltration of tar vapor into the ore-pores. As a result, carbon deposited near the surface occupied the pores and penetration of the tar vapor was blocked by the carbon. Observation of carbon morphology by Raman spectroscopy revealed that the deposited carbon was amorphous.

Hosokai et al. conducted kinetic analysis for reduction reaction of CVI ore [36]. They tried to use CVI ore produced from goethite ore and biomass, mixture of reagent Fe_3O_4 and carbon black, and mixture of reagent Fe_3O_4 and coke. Reduction started at around 1100℃ and 900℃ when Fe_3O_4/carbon black and Fe_3O_4/coke

were used. The CVI ore, however, started to reduce at much lower temperature; approximately 700℃. The reduction at lower temperature was said to be the effect of close contact between goethite ore and carbon.

CVI ore is very attractive material for ironmaking because of the lower reduction temperature. As is mentioned above, a lot of study has been conducted to increase the amount of carbon in the CVI ore, however, only 5wt% is the maximum carbon content. This carbon amount is not enough for perfect reduction to metallic iron.

To overcome the defect of the CVI ore, carbon infiltrated goethite ore which is prepared from mixture of tar and goethite ore [44-46]. Maximum of 50 mass% of carbon is reachable in goethite ore by this method [46]. This carbon content is enough for the goethite ore to be reduced completely.

1-5. Purpose of this study

The iron and steel industry is one of the biggest industry in the world, however, the industry has three problems about resource, environment, and energy. The amount of utilization of high-grade iron ore has been increasing, resulting in degradation of the ore. The CO_2 emissions account for around 9% of the total emissions in the world. Large amount of high-temperature waste heat is emitted without effective utilization.

The goethite ore, one of the alternative iron ore in the iron and steel industry, contained 10% of combined water (CW). The CW in the goethite ore needs to be removed by calcination; this is disadvantage of the goethite usage because additional energy is essential for the calcination process. However, the goethite ore has an interesting property to become nanoporous material after mild calcination. This nanoporous goethite ore is promising as reaction field to solve the environmental and energetic problems in the iron and steel industry.

To solve the environmental and energetic problems in the iron and steel industry using this goethite-based ore, two solutions are proposed in this thesis: (1) Ni-containing goethite ore as a catalyst for the dry reforming of methane and (2) fast combustion synthesis ironmaking of carbon infiltrated goethite ore.

This thesis consists of five chapters as follows:

Chapter 1 presents General Introduction of this study.

Chapter 2 and 3 describe observation of the catalytic performance of Ni-

containing goethite-based ore in the laterite soil. In chapter 2, some natural goethite-based ores containing different amounts of Ni were utilized in the catalytic tests for the dry reforming of methane and their catalytic performances were compared. The effect of Ni in the ores was mainly discussed in this chapter.

In chapter 3, the detailed catalytic properties of the Ni-containing goethite ore were observed. The goethite ore contains a lot of Fe components and they easily change their composition (Fe_2O_3, Fe_3O_4, FeO, and Fe) during the catalytic tests. The state of the goethite ore was controlled during the catalytic test and the catalytic properties were observed in detail in this chapter.

Chapter 4 describes a fast ironmaking process, "combustion synthesis" using nanoporous goethite ore. Carbon-infiltrated goethite ore was synthesized from tar-based solution and mildly-calcined goethite ore and it was reduced by rapid heating in an oxygen atmosphere.

In Chapter 4, theoretically possible conditions of the combustion synthesis reaction were mainly discussed from the viewpoint of the adiabatic temperature. Detailed calculations were taken place by a numerical software. The combustion synthesis ironmaking was experimentally conducted using carbon infiltrated goethite ore prepared via tar impregnation method. The reaction mechanism of the combustion synthesis reaction was mainly discussed here.

Chapter 5 presents the General conclusion of this thesis.

REFERENCES

[1] International Iron and Steel Institute, “Steel Statistical Yearbook”.

[2] International Monetary Fund, “Primary Commodity Prices”.

[3] International Energy Agency (IEA), “Coal Information”.

[4] United States Bureau of Mines (USGS), “USGS Minerals Yearbook”.

[5] A.V. Todorut, D. Cirtina, L.M. Cirtina, Metalurgija 56 (2017).

[6] IEA, “CO_2 emissions from fuel combustion 2016”.

[7] IEA, “Tracking Industrial Energy Efficiency and CO_2 emissions” (2007).

[8] H. Nogami, J. Yagi, S. Kitamura, P.R. Austin, ISIJ International 46 (2006).

[9] IEA, “Worldwide Trends in Energy Use and Efficiency, Key Insights from IEA Indicator Analysis”.

[10] T. Akiyama, J. Yagi, Tetsu-To-Hagane 82 (1996).

[11] G. Saito, T. Nomura, N. Sakaguchi, T. Akiyama, ISIJ International 56 (2016).

[12] F. Watari, J.V. Landuyt, P. Delavignette, S. Amelinckx, Journal of Solid State Chemistry 29 (1979).

[13] F. Watari, P. Delavignette, S. Amelinckx, Journal of Solid State Chemistry 29 (1979).

[14] F. Watari, P. Delavignette, J.V. Landuyt, S. Amelinckx, Journal of Solid State Chemistry 48 (1983).

[15] H. Naono, R. Fujiwara, Journal of Colloid and Interface Science 73 (1979).

[16] H. Naono, K. Nakai, T. Sueyoshi, H. Yagi, Journal of Colloid and Interface Science 120 (1987).

[17] J.L. Rendon, J. Cornejo, P. Arambarri, C.J. Serna, Journal of Colloid and

Interface Science 92 (1983).

[18] Japan Oil, Gas and Metals National Corporation (JOGMEC), “Metallic Resources Report 2013” (in Japanese).

[19] G.M. Mudd, Ore Geology Reviews 38 (2010).

[20] H. Tsuji, doctoral dissertation of Kyoto University (2013), DOI: 10.14989/doctor.r12765 (in Japanese).

[21] M. Kiyomiya, M. Kawai, Atmospheric environment 13 (1979) 559-561.

[22] M. L. Cubeiro, M.R. Goldwasser, M.J. Perez Zurita, C. Franco, F. Gonzalez-Jimenez, E, Jaimes, Hyperfine Interactions 93 (1994) 1831-1835.

[23] N. Tsubouchi, H. Hashimoto, Y. Otsuka, Catalysis Letters 105 (2005).

[24] T. Akiyama, K. Oikawa, T. Shimada, E. Kasai, J. Yagi, ISIJ International 40 (2000).

[25] M. Garcia-Dieguez, I.S. Pieta, M.C. Herrera, M.A. Larrubia, L.J. Alemany, Journal of Catalysts 270 (2010).

[26] D. Pakhare, J. Spivey, Chemical Society Review 22 (2014).

[27] Tokyo Kagaku Houjin Co., Ltd., Kagaku-jiten (1999) (in Japanese).

[28] K. Tozawa, Tetsu To Hagane 79 (1992).

[29] NTS CO., Ltd., Syokubai Chousei Handbook (2011) (in Japanese).

[30] F. Habashi, Hydrometallurgy 79 (2005).

[31] J.H. Kim, D.J. Suh, T.J. Park, K.L. Kim, Applied Catalysis A: General 197 (2000).

[32] Private communication with Professor Masakata Shimizu, Kyusyu University.

[33] R.B. Cahyono, doctoral dissertation of Hokkaido University (2015), DOI:

10.14943/doctoral.k11881

[34] Y. Hata, H. Purwanto, S. Hosokai, J. Hayashi, Y. Kashiwaya, and T.Akiyama, Energy & Fuels, 23(2), (2009), pp.1128-1131.

[35] A. N. Rozhan, R. B. Cahyono, N. Yasuda, T. Nomura, S. Hosokai, H. Purwanto, T. Akiyama, Energy and Fuels, 26 (2012), pp.7340-7346.

[36] S. Hosokai, K. Matsui, N. Okinaka, K. Ohno, M. Shimizu, and T. Akiyama, Energy Fuels, 26 (2012), pp. 7274–7279.

[37] R. B. Cahyono, A. N. Rozhan, N. Yasuda, T. Nomura, S. Hosokai, Y. Kashiwaya, T. Akiyama, Fuel Processing Technology 113, (2013), pp.84-89.

[38] R. B. Cahyono, A. N. Rozhan, N. Yasuda, T. Nomura, H. Purwanto, T. Akiyama, Energy Fuels 27 (2013), pp 2687–2692.

[39] R.B. Cahyono, N. Yasuda, T. Nomura, T. Akiyama, Fuel Processing Technology 119 (2014), pp. 272-277

[40] R. B. Cahyono, G. Saito, N. Yasuda, T. Nomura, and T. Akiyama, Energy Fuels, 2014, 28 (3), pp. 2129–2134

[41] R.B. Cahyono, N. Yasuda, T. Nomura, T. Akiyama, ISIJ International 55, No. 2 (2015), pp. 428-435.

[42] T. Nomura, R. B. Cahyono, T. Akiyama, Journal of Sustainable Metallurgy, 1 (2015), pp.115-125.

[43] A. Kurniawan, K. Abe, T. Nomura, and T. Akiyama, Energy Fuels, in press.

[44] Y. Mochizuki, N. Tsuboushi, T. Akiyama, Fuel Processing Technology 138 (2015).

[45] Y. Mochizuki, M. Nishio, N. Tsuboushi, T. Akiyama, Fuel Processing

Technology 142 (2016).

[46] Y. Mochizuki, M. Nishio, J. Ma, N. Tsuboushi, T. Akiyama, Energy and Fuels 30 (2016).

Chapter 2

Ni-containing Goethite Ore as a Catalyst for the Dry Reforming of Methane

2-1. Introduction

The iron and steel industry has problems about unutilized high-temperature waste heat and CO_2 emission. Large amounts of high-temperature waste heat above 873 K from the steel industry, such as blast furnace slag and coke oven gas, are discharged without effective utilization [1]. Furthermore, CO_2 emission from the steel industry was estimated to account for approximately 15% of total emission in Japan [2]. The emission of high-temperature waste heat and CO_2 is not good for energy utilization and environment.

In an attempt to utilize high-temperature waste heat effectively and reduce CO_2 emissions from the steel industry, we focused on the dry reforming reaction of methane, expressed below.

$$CH_4 + CO_2 \rightarrow 2H_2 + 2CO \quad (\Delta H° = +247 \text{ kJ mol}^{-1} \text{ at } 298 \text{ K}) \quad (2\text{-}1)$$

Akiyama et al. theoretically showed that the dry reforming reaction can occur using high-temperature waste heat and that thermal energy is converted to chemical energy in the production of H_2 and CO [3]. It is therefore an appropriate method for the utilization of high-temperature waste heat and reduction of CO_2 emission.

The dry reforming of methane is a catalytic reaction and a lot of metal-based catalysts, such as Ni [4-8], Co [8], Pt [9,10], Rh [11], Ir [11], and Ru [12] have been investigated for use in the dry reforming reaction, with particular attention focused on Ni-based catalysts. These metal-based catalysts show good catalytic performance, however, they have some problems; (i) it is expensive because they consist of rare metals, (ii) metal particles on the catalysts should be nanosize and a lot of processes are needed such as impregnation, drying, and calcination, and (iii) when carbon is deposited on the surface of the catalysts, the catalytic performance decreases and they cannot be used anymore.

Ni-based catalysts show high catalytic performances in the dry-reforming reaction, so we focused on Ni-containing goethite ore as a catalyst for the dry reforming of methane. The examples of the composition of the Ni-containing goethite ores from Indonesia [14-17] and the Philippines [18-21] are shown in Table 2-1.

Table 2-1 Examples of the compositions of Ni-containing goethite ores in laterite soil. Ore 1-4 and ore 5-8 are from Indonesian and the Philippine, respectively.

*T-Fe and CW means total Fe and combined water.

	Compositions (wt%)											
	T-Fe	NiO	Al_2O_3	SiO_2	CaO	MgO	MnO	Na_2O	TiO_2	Cr_2O_3	Co_3O_4	CW
Ore 1[19]	44.2-46.2	0.68-1.1	8.8-12.0	2.8-3.2	0.03	0.4-0.7	0.32-0.36	0.1-0.5	0.19-0.45	4.99-6.58	-	13.5-14.0
Ore 2[20]	50.9	0.38	8.8	9.7	0.03	0.3	-	-	-	5.90	0.03	11.0
Ore 3[21]	49.9	1.0	7.1	6.3	-	2.0	0.58	-	-	3.14	0.11	-
Ore 4[22]	41.0	1.2	6.5	12.6	0.3	4.7	0.82	-	-	2.86	0.12	13.2
Ore 5[23]	48.3	1.32	3.5	3.2	0.20	1.6	1.02	-	-	3.79	0.13	10.7
Ore 6[24]	40.5	2.0	8.5	9.2	0.0	1.7	2.8	0.0	-	2.3	0.3	-
Ore 7[25]	45.4	1.39	5.3	6.9	0.06	1.3	1.87	-	-	4.34	0.12	-
Ore 8[26]	37.0-39.7	0.72-1.11	5.7-6.1	2.6-3.2	0.02-0.03	0.0-0.2	0.12-0.43	0.0-0.1	0.06-0.14	1.24-2.25	0.06-0.08	-

Goethite ores in the laterite soil contain approximately 1 wt% Ni and 10 wt% CW. The CW of the goethite ore is easily removed from the ore and FeOOH changes its form to porous Fe_2O_3 (eq. 2-2) which can then be used as a catalyst owing to its high surface area. Naono et al. reported that FeOOH decomposes into nanoporous Fe_2O_3 via dehydration when heated at approximately 573 K [13].

$$2FeOOH \rightarrow Fe_2O_3 + H_2O \qquad (2\text{-}2)$$

In addition to the possibility as a catalyst, Ni-containing goethite ore has some good points compared with conventional metal-based catalysts; (i) The goethite ore as a catalyst is much cheaper material since it is natural ore, (ii) it can be synthesized via more simple process (only dehydration) than conventional catalysts and the

goethite ore itself has nanostructure after dehydration, and (iii) the goethite ore can be recycled as iron and nickel sources after carbon deposition.

Carbon deposition on dehydrated nanoporous iron ore, on the other hand, have a good effect on the iron ore from the viewpoint of iron-making. Hata et al. deposited carbon on porous iron ore from pyrolyzed gas of biomass and obtained composite of carbon and partially reduced iron ore (Fe_3O_4) [22]. Hosokai et al. revealed that the composite shows faster reduction rate compared with mixture of reagent Fe_3O_4 and coke [23]. It is attractive to utilize nanoporous iron ore as a catalyst because they can be reused as iron resources after carbon deactivation.

In spite of their attracted characteristics, utilization of Ni-containing goethite ores as catalysts has not been reported, therefore, in this study, we investigated the catalytic properties of iron ores (laterite and non-laterite) containing different amounts of Ni for the dry-reforming reaction of methane and identified the effect of Ni in the goethite ore by examining its structure and comparing with non-Ni and Ni-supported iron ores. We also researched the porous structure, the degree of reduction, and the amount of carbon deposition of the iron ores.

2-2. Materials and experimental methods

2-2-1. Ni-containing goethite ores

Four goetihte-based catalysts, three of which were produced by dehydrating natural goethite ores and the fourth was obtained by supporting Ni on the goethite ore, were used for the catalytic tests. Table 2-2 shows the composition of the goethite ores (LN, SN, and NN ores). LN (large amount of Ni) ore from Gaboc (Philippines), SN (small amount of Ni) ore from Sebuku (Indonesia), and NN (no nickel) ore from Hamersley (Australia) contain 1.18, 0.30, and 0 wt-%Ni, respectively.

Table 2-2. Compositions of the ores in this study.

	Compositions (wt%)										
	T-Fe	Ni	Cr_2O_3	Al_2O_3	SiO_2	CaO	MnO	MgO	TiO_2	Co	CW
LN ore	47.99	1.18	3.32	-	2.12	-	1.26	0.47	0.10	0.10	12.6
SN ore	50.88	0.30	5.90	8.84	9.66	0.03	-	0.31	-	0.03	11.0
NN ore	58.65	-	-	1.55	4.53	0.05	-	-	-	-	8.62

*T-Fe and CW means total Fe and combined water.

2-2-2. Preparation of ore catalysts

LN, SN, and NN ores were crushed to 300–1000 μm size and were dehydrated at 773 K for 4 h in a muffle furnace to afford natural goetihte ore catalysts. The

Ni-supported goetihte ore (1.0 wt%Ni) was prepared from the NN ore and $Ni(NO_3)_2 \cdot 6H_2O$ aqueous solution to confirm the effect of nickel in the ores. The NN ore (before dehydration) was added to $Ni(NO_3)_2 \cdot 6H_2O$ aqueous solution and the solution was evaporated to dryness at 313 K (below the melting point of $Ni(NO_3)_2 \cdot 6H_2O$). After drying at 383 K under vacuum, it was then calcined at 773 K for 4 h.

2-2-3. Catalytic tests

Catalytic tests were performed in a catalytic packed-bed reactor. A schematic image of the equipment is shown in Figure 2-1. The input gases flowed through a quartz tube (φ6 mm × 554 mm) and passed over a catalytic zone containing an iron ore catalyst. The temperature of the catalytic zone was kept at a programmed temperature by a controlled system using a thermocouple which was placed just below the quartz wool to secure the ore catalysts.

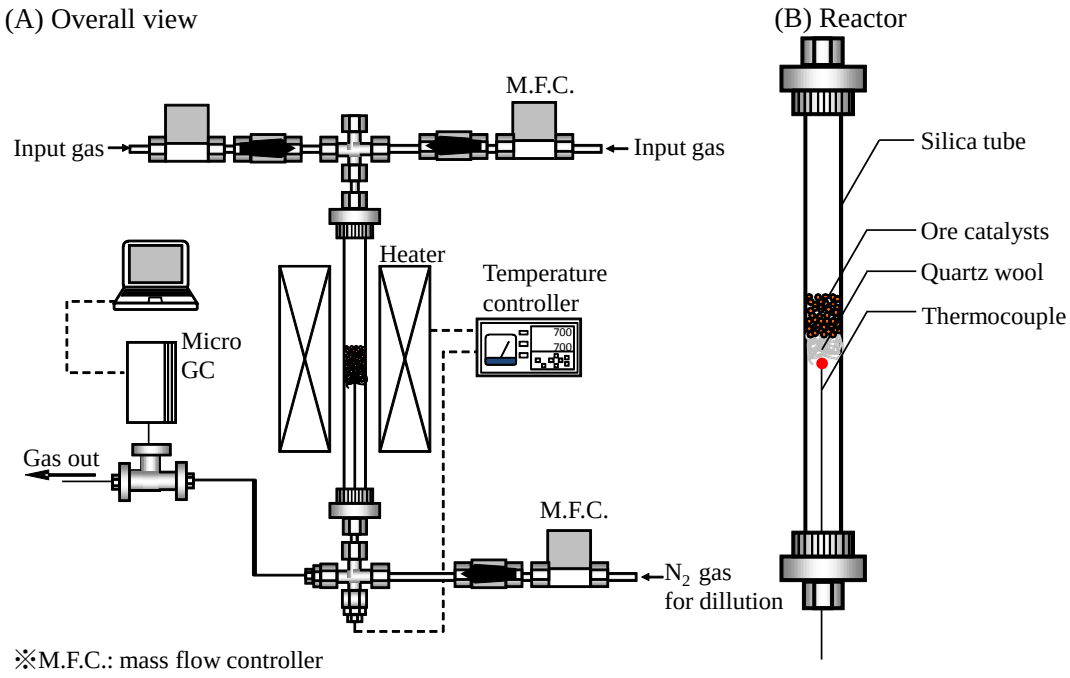

Figure 2-1 Schematic diagram of the apparatus for the catalytic tests.

First, we prepared dehydrated LN, SN, NN, and Ni-supported NN ores. Reagent Fe (99.9%, 150 μm pass) was also used as a reference catalyst. 1.0 g ores or reagent were placed in the quartz tube. The ores were then heated to a target temperature (973–1173 K) at rate of 10 K/min under a N_2 flow. Just before the target temperature was reached, the N_2 flow was stopped and CH_4 and CO_2 flow began. The flow rates of the gases were controlled by mass flow controllers. The catalytic tests were performed for 1 h and the composition of the product gases was measured with a gas chromatograph (Agilent 3000, INFICON Co., Ltd., Yokohama, Japan) every 5 min. After the catalytic tests, the flow of CH_4 and CO_2

was stopped and N_2 was again flowed until the iron ore had cooled to room temperature.

2-2-4. Properties of the catalysts

Pore structure, phase identification, and surface observation measurements of the iron ores were conducted before and after the catalytic tests. The pore structures and surface areas of the ores were estimated by nitrogen gas adsorption measurements (Autosorb 6AG, Yuasa Ionics Co. Ltd., Osaka, Japan). The specific surface areas of the ores were evaluated by the Brunauer-Emmett-Teller (BET) model and pore size distribution was calculated using the Barrett-Joyner-Halenda (BJH) method. Before and after the catalytic tests, the phase identification of the ores was conducted using X-ray diffractometry (XRD; Miniflex, Rigaku, Tokyo, Japan), scanning electron microscopy (SEM; JSM-7001FA, JEOL, Tokyo, Japan), and transmission electron microscopy (TEM; JEM-2010F, JEOL, Tokyo, Japan) with energy dispersive X-ray spectroscopy (EDS). Carbon amount on the catalysts after catalytic tests were evaluated using a CHN/O/S elemental analyzer (CE-440; EAI, United States).

2-3. Results and discussion

Figure 2-2 shows the XRD patterns of the iron ores before and after dehydration. The results indicated that the iron ores mainly contained FeOOH (some Fe_2O_3 in SN and NN ores) before dehydration and Fe_2O_3 after dehydration. This meant that the decomposition reaction of CW ($2FeOOH \rightarrow Fe_2O_3 + H_2O$) occurred in all iron ores at 773 K.

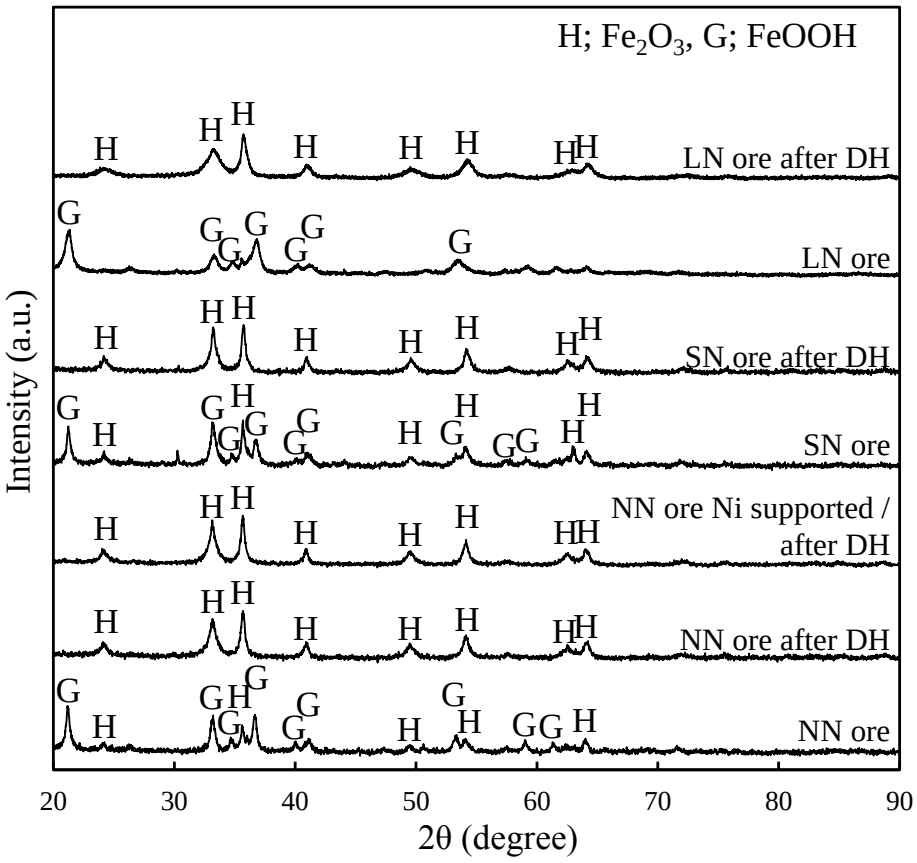

Figure 2-2 XRD patterns of the ores before and after dehydration at 773 K for 4 h.

Figure 2-3 shows the CO_2 conversion ratios of LN, SN, NN, and Ni-supported NN (1 wt% Ni) ores during the catalytic tests at 1173 K. The CO_2 conversion ratio is defined by the following equation:

$$CO_2 \text{conversion ratio} = \frac{\text{input flow rate of } CO_2 - \text{output flow rate of } CO_2}{\text{input flow rate of } CO_2} \quad (2\text{-}3)$$

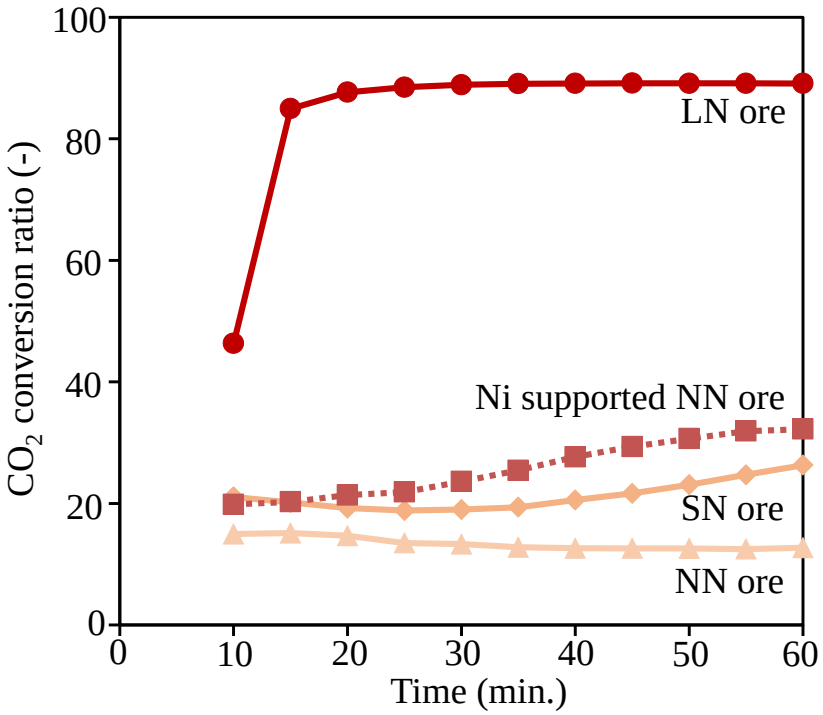

Figure 2-3 CO_2 conversion ratio ([input flow rate of CO_2 – output flow rate of CO_2]/input flow rate of CO_2) during the catalytic tests using LN, SN, NN, and Ni-supported NN ores at 1173 K for 1 h.

The LN ore had the highest CO_2 conversion ratio, followed by Ni-supported NN, SN, and NN ores. This order corresponds to the Ni content of the iron ores, with ores containing larger amounts of Ni showing higher CO_2 conversion ratios. However, the CO_2 conversion ratio of the LN ore was much higher than that of the Ni-supported NN ore, despite the fact that they contained almost the same amount of Ni.

Figure 2-4 shows the adsorption isotherms of the LN, SN, and NN ores after the DH at 773 K for 4 h and Figure 2-5 shows the typical types of the isotherms drawn by Sing et al. [24]. In Figure 2-5, general six types of isotherms (left) and four types of isotherms which have hysteresis (right) are drawn. The isotherms obtained from SN and NN ores resembled H4-type isotherm in Figure 2-5, implying slit-like mesopores existed in the dehydrated SN and NN ores [24]. The isotherm obtained from LN ore also showed small hysteresis like H4 isotherm (slit-like mesopores) but the overview was like III-type isotherm in Figure 2-5. The III-type isotherm indicates existence of macropores [24]. Those meant that the pores of the LN ore consisted of two-types of pores; slit-like mesopores and macropores. Figure 2-6 shows the pore size distributions and BET surface areas of the iron ores before and after dehydration at 773 K for 4 h. Mesopores of 4 nm diameter were mainly formed during the dehydration process and all iron ores had higher surface areas (58.9–101 $m^2\ g^{-1}$) after dehydration due to the formation of nanopores by detachment of CW.

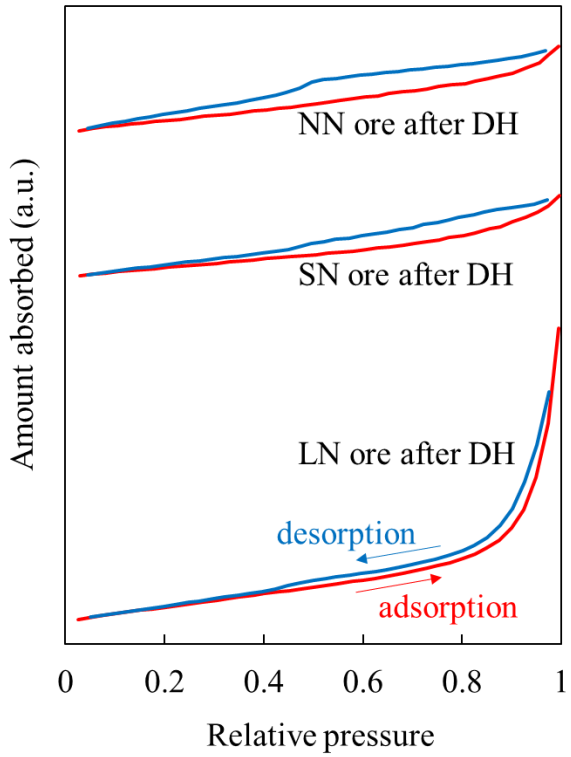

Figure 2-4 Adsorption isotherms of the LN, SN, and NN ore after DH at 773 K for 4 h.

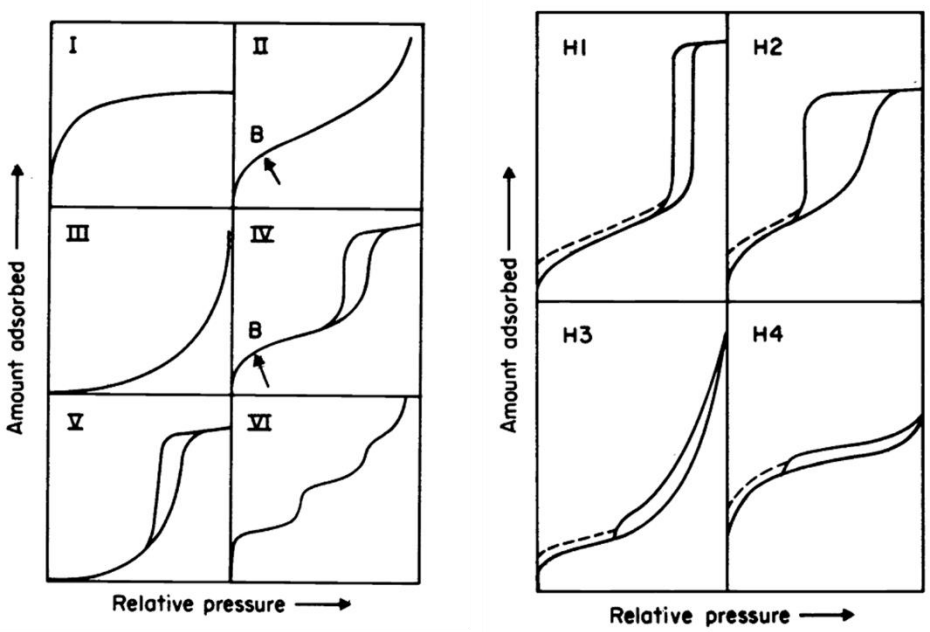

Figure 2-5 Types of physisorption isotherms and hysteresis loops [24]

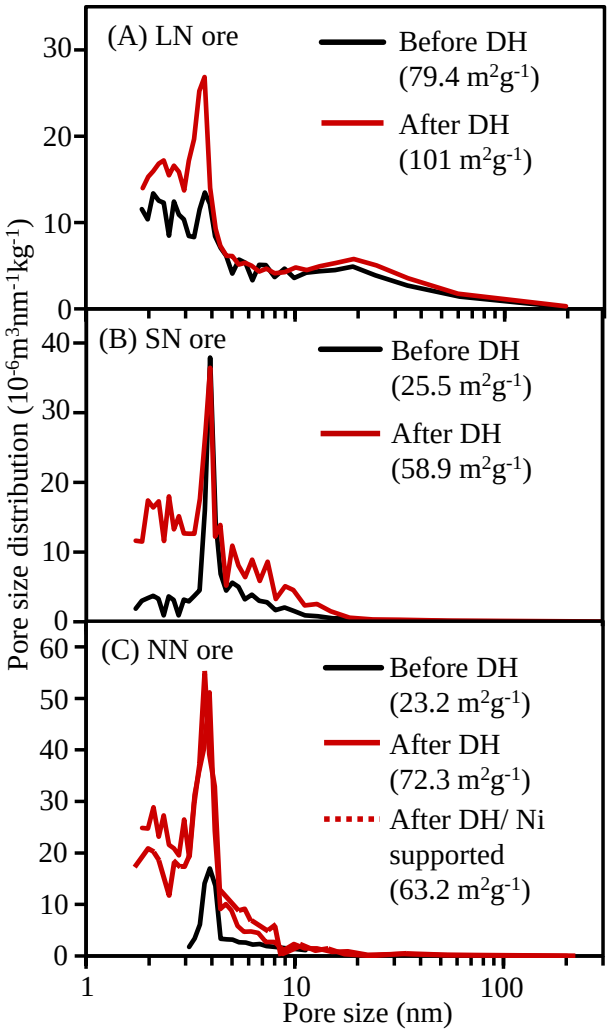

Figure 2-6 Pore size distributions and BET surface areas of the LN, SN, and NN ores before and after dehydration at 773 K for 4 h.

Figure 2-7 shows the SEM images of LN and SN ores before and after the dehydration process. The LN ore had a high surface area (79.4 $m^2 g^{-1}$) even before dehydration as it contained many pores (micropore, mesopore, and macropore) and the surface area increased further after dehydration (101 $m^2 g^{-1}$). A lot of cracks were observed on the surface of the LN ore which might be related to the

macropores shown in Figures 2-4 and 2-6. The SN ore had a lower surface area (25.5 $m^2 g^{-1}$) than the LN ore before dehydration as it contained fewer pores. After dehydration, however, a lot of nanopores were observed in the SN ore. The BET surface area of the LN ore after dehydration (101 $m^2 g^{-1}$) was much higher than that of the Ni-supported NN ore after dehydration (63.2 $m^2 g^{-1}$).

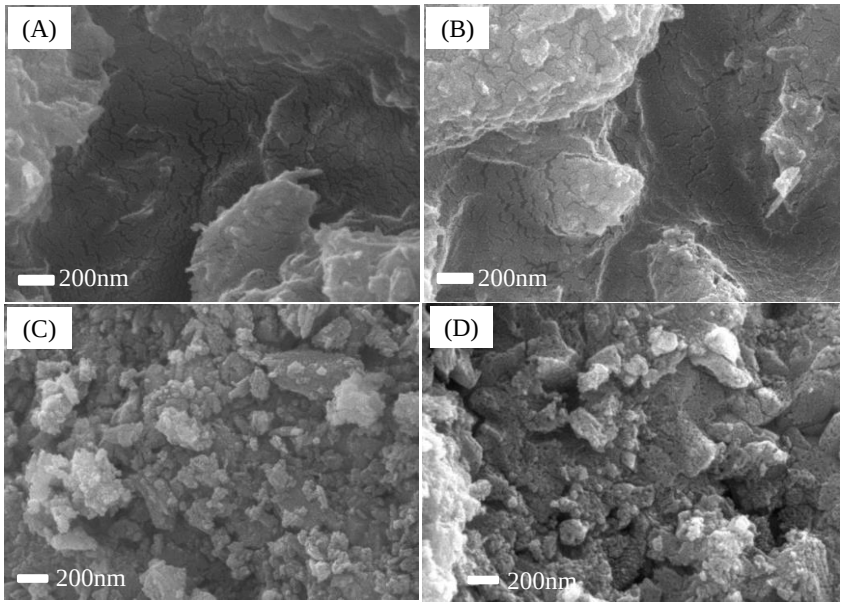

Figure 2-7 SEM images of (A); LN ore before dehydration (DH), (B); LN ore after DH, (C); SN ore before DH, and (D); SN ore after DH.

Fig. 2-8 shows the TEM images and EDS spectra of Ni-supported NN and LN ores before and after catalytic tests at 1173 K. We conducted EDS point analysis at certain points in these ores and found that Ni peaks could be detected everywhere in the LN ore, but only in a small part of the Ni-supported NN ore. This indicated

that Ni existed as fine particles in the LN ore, but was of larger particle size (around 20 nm, Fig. 2-8) in the Ni-supported NN ore. According Tang and Valix, Ni exists as (Fe, Ni)O(OH) in iron matrix of laterite ores, meaning Ni disperses at the atomic level [25]. This higher dispersion means a higher surface area of Ni.

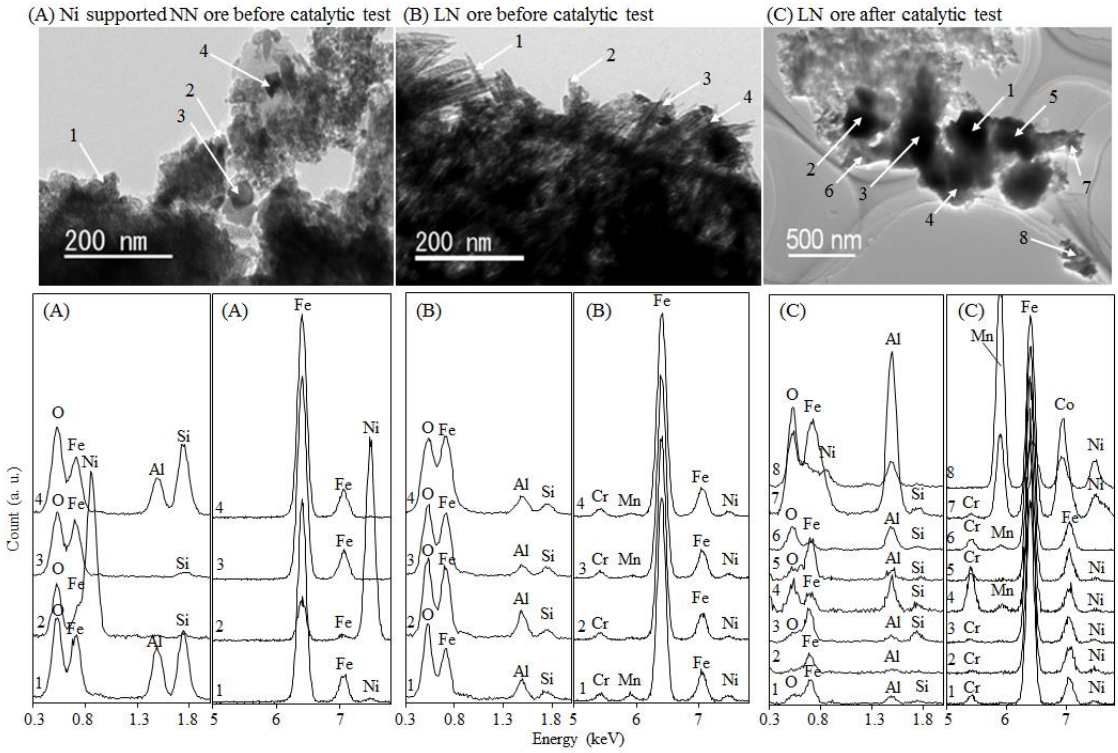

Figure 2-8 TEM images of (A); Ni-supported NN ore before the catalytic test, (B); LN ore before the catalytic test, and (C); LN ore after the catalytic test at 1173 K for 1 h, and EDS point analyses of each point in TEM images.

LN ore has higher surface area and higher Ni dispersion, resulting in the higher catalytic performance of the LN ore than that of the Ni-supported NN ore. Especially, higher Ni dispersion contributed more to higher catalytic performance because it is Ni to show good catalytic performance for the dry reforming reaction. After the catalytic test, some Ni was agglomerated in the LN ore but it still contained more highly dispersed Ni particles than the Ni-supported NN ore.

Figure 2-9 shows the composition of CH_4, CO_2, H_2, and CO gas during the catalytic tests for LN ore. In the absence of catalyst, the dry-reforming reaction barely proceeded and the output gas contained little H_2 and CO. On the other hand, using LN ore as the catalyst, the decomposition of CO_2 and CH_4, and production of H_2 and CO increased. This indicated that LN ore has good catalytic properties for the dry reforming reaction. At higher temperatures, the amount of decomposed CO_2 and CH_4, and produced H_2 and CO increased further.

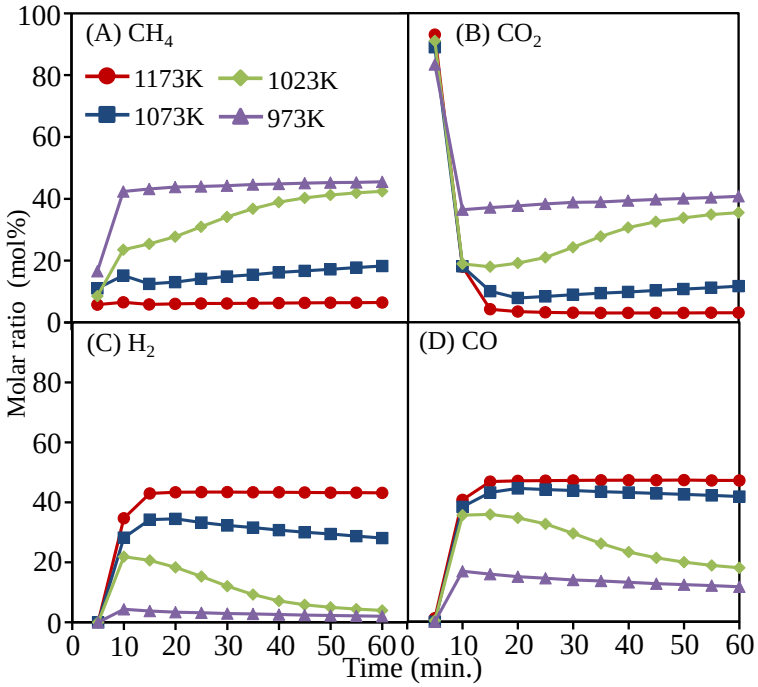

Figure 2-9 Gas composition of (A) CH_4, (B) CO_2, (C) H_2, and (D) CO during the catalytic tests using LN ore.

Figure 2-10 (A) shows the XRD patterns of the LN ore before and after the catalytic tests. Before the catalytic tests, iron existed as Fe_2O_3 (LN ore after DH in Figure 2-2). During the catalytic tests, Fe_2O_3 in the LN ore was reduced to Fe_3O_4, FeO, or Fe at all temperatures. Ni oxide in LN ore was also reduced at higher temperatures. Figure 2-10 (B) shows XRD patterns from 43 to 45 degrees. Ni content in LN ore was very small, that is why slower scanning speed was used for Figure 2-4 (B) to detect Ni components. Nickel existed as oxide during the catalytic tests at 973 and 1023 K and changed its form to metal at 1073 and 1123 K. The iron ore showed

more reduction at higher temperatures and metallic iron and nickel were produced above 1073 K (reduction proceeded only to Fe_3O_4 at lower temperatures). The differences in the catalytic performance and reduction ratio of iron oxides at certain temperatures were evaluated as follows. At first, the dry reforming reaction rate increased with rising temperature and more reducing gases (H_2 and CO) were generated. Then, the reducing gases passed through the catalytic zone and reduced oxides, for instance, Fe and Ni oxides. These reduced metal components had even higher catalytic properties than oxides and much more reducing gases were produced. Low H_2/CO ratio at lower temperature was considered to be the effect of the reverse water gas shift reaction (RWGSR). The reaction equation of RWGSR is as follows:

$$H_2 + CO_2 \rightarrow CO + H_2O \quad (\Delta H° = +41 \text{ kJ mol}^{-1} \text{ at } 298 \text{ K}) \quad (2\text{-}4)$$

Some articles have reported that the dry reforming reaction and the RWGSR occurred at the same time at comparatively low temperature in case of using Ni catalysts [26, 27].

Figure 2-11 and Table 2-3 show the SEM images and BET surface area of the LN ore after the catalytic tests, respectively. Pores and cracks can be observed in the LN ore before the catalytic tests (SEM images in Figure 2-7), but not after (Figure 2-11). The surface area of the LN ore drastically decreased after the catalytic tests, particularly at higher temperatures (101 and 4.20 $m^2 g^{-1}$ before and after catalytic tests at 1173 K, respectively). At higher temperature, LN ore had

metal components (Fe and Ni) and they were more easily sintered than oxides.

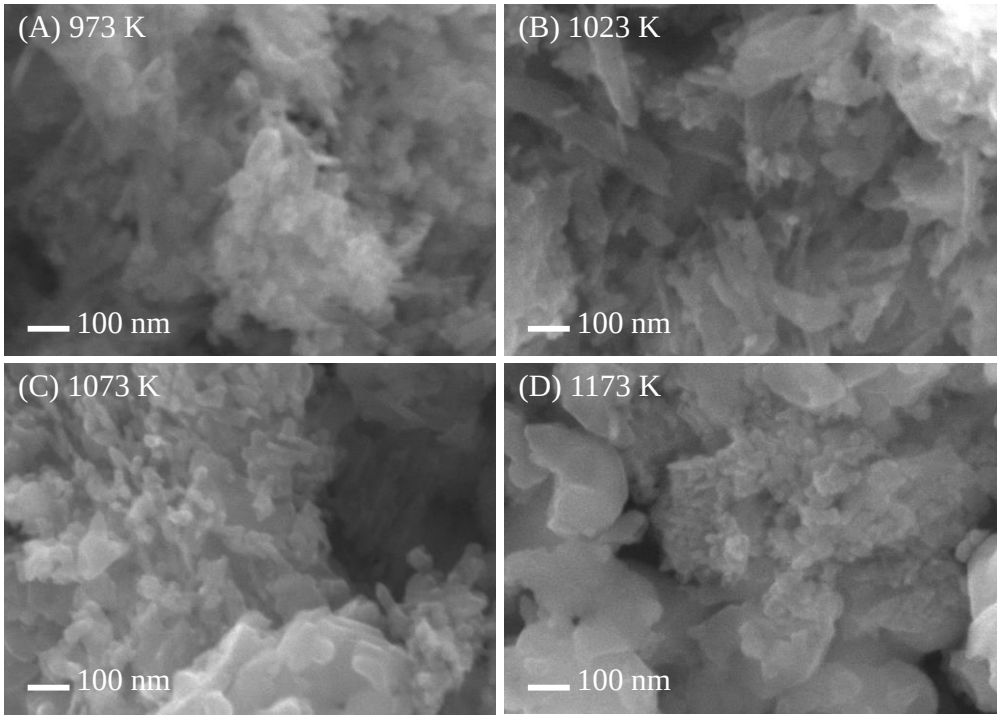

Figure 2-11 SEM images of LN ore after the catalytic tests at (A) 973 K, (B) 1023 K, (C) 1073 K, and (D) 1173 K.

Table 2-3. BET surface areas of LN ore before and after catalytic tests.

	LN ore before catalytic tests	LN ore after catalytic tests			
		973 K	1023 K	1073 K	1173 K
Surface area (m^2 g^{-1})	101	35.4	22.9	12.1	4.20

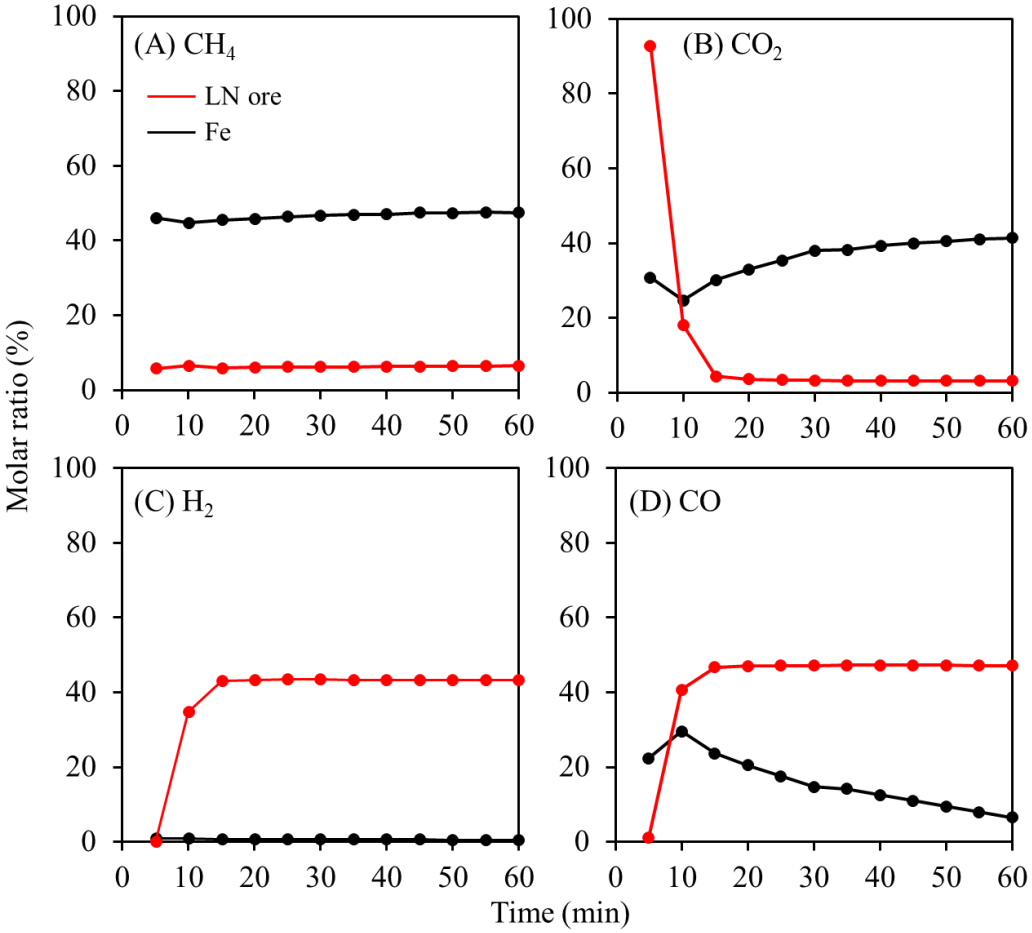

Figure 2-12 Gas composition of (A) CH_4, (B) CO_2, (C) H_2, and (D) CO during the catalytic tests using reagent Fe and LN ore.

Figure 2-12 shows the composition of CH_4, CO_2, H_2, and CO gas during the catalytic tests for reagent Fe_3O_4, reagent FeO, reagent Fe, and LN ore. CH_4 decomposition and H_2 formation were not observed on the iron-based reagents, implying that metallic iron and iron oxides had almost no catalytic effect in the dry reforming reaction. Only CO_2 decomposition and CO formation were observed on the reagent FeO and Fe. That is because the FeO and Fe were oxidized by the input

CO_2 gas.

$$Fe + CO_2 \rightarrow FeO + CO \qquad (2\text{-}5)$$

The Ni-containing goethite ore was utilized as a catalyst for the dry reforming of methane in this study. Ni in the goethite ore effectively worked in the dry-reforming reaction, however, metallic iron and iron oxides had less catalytic activity in this reaction. The Ni in the goetihte ore homogeneously distributed compared with the Ni-supported ore, resulting in higher catalytic performance.

2-4. Summary

We utilized Ni-containing goethite ores (LN, SN, and NN ores) and Ni-supported ore (Ni-supported NN ore) as catalysts for the dry reforming reaction of methane ($CH_4 + CO_2 \rightarrow 2H_2 + 2CO$) by conducting catalytic tests under CH_4 and CO_2 flow (CH_4:CO_2 = 1:1) at 973–1173 K.

All goethite ores were successfully dehydrated at 773 K for 4 h and FeOOH became Fe_2O_3 and slit-like mesopores were generated in the ores, however, the catalytic tests at higher temperatures drastically reduce their surface areas due to sintering. The CO_2 conversion ratio of the LN ore was much higher than that of Ni-supported NN ore despite the fact that they contained almost the same amount of Ni. This is due to higher dispersion of Ni in the LN ore. Ni existed quite finely in the LN ore, but had a much larger particle size in the Ni-supported NN ore. Smaller Ni particles have a higher surface area, resulting in the higher catalytic performance of the LN ore.

With LN ore as the catalyst, at higher temperatures the amount of decomposed CO_2 and CH_4, and produced H_2 and CO increased. The reduction of iron ores proceeded more at higher temperatures and metallic iron and nickel were produced above 1073 K; reduction did not progress past Fe_3O_4 at lower temperatures. This is due to the higher amounts of reducing gas (H_2 and CO) at higher temperatures. In the goetihte ore catalyst, only Ni effectively worked as catalyst in the dry reforming reaction; iron components showed much lower catalytic activity.

REFERENCES

[1] Akiyama, T; Yagi, J., Tetsu-to-Hagane **1996**, 82, 177-184 (in Japanese).

[2] Gielen, D; Moriguchi, Y., Energy Policy **2002**, 30, 849-863.

[3] Akiyama, T; Oikawa, K; Shimada, T; Kasai, E; Yagi, J., ISIJ Int. **2000**, 40, 288-291.

[4] Wang, S; Lu, G.Q.M., Appl. Catal. B **1998**, 16, 269-277.

[5] Wang, S; Lu, G.Q.M., Appl. Catal. B **1998**, 19, 267-277.

[6] Wang, S; Lu, G.Q.M., Energy & Fuels **1998**, 12, 248-256.

[7] Montoya, J. A.; Romero-Pascual, E.; Gimon, C.; Del Angel, P.; Monzon, A., Catal. Today **2000**, 63, 71-85.

[8] Fan, M.S.; Abdullah, A.Z.; Bhatia, S., Appl. Catal. B **2010**, 100, 365-377.

[9] Damyanova, S.; Pawelec, B.; Arishtirova, K.; Martinez Huerta, M.V.; Fierro, J.L.G., Appl. Catal. B **2009**, 89, 149-159.

[10] Stagg-Williams, S. M.; Noronha, F. B.; Fendley, G.; Resasco, D. E., J. Catal. **2000**, 194, 240-249.

[11] Mark, M. F.; Maier, W. F., J. Catal. **1996**, 164, 122-130.

[12] Bradford, M. C. J.; Vannice, M. A., J. Catal. **1999**, 183, 69-75.

[13] Naono, H; Fujiwara, R J., Colloid and Interface Sci. **1980**, 73, 406-415.

[14] Fu, W.; Yang, J.; Yang, M.; Pang, B.; Liu, X.; Niu, H.; Huang, X., J. Asian Earth Sci. **2014**, 93, 74-88.

[15] Purwanto, H.; Shimada, T.; Takahashi, R.; Yagi, J., ISIJ Int. **2002**, 42, 243-247.

[16] Wang, B.; Guo, Q.; Wei, G.; Zhang, P.; Qu, J.; Qi, T., Hydrometall. **2012**, 129-130, 7-13.

[17] Zhu, D.; Cui, Y.; Hapugoda, S.; Vining, K.; Pan, J., Trans. Nonferrous Met. Soc. China **2012**, 22, 907-916.

[18] Ma, B.; Wang, C.; Yang, W.; Chen, Y.; Yang, B., Int. J. Miner. Process. **2013**, 124, 42-49.

[19] Fan, R.; Gerson, A. R., Geochim. Cosmochim. Acta **2011**, 75, 6400-6415.

[20] Ogura, Y.; Murata, K.; Iwai, M., Chemical Geology **1987**, 60, 259-271.

[21] Andersen, J.; Rollinson, G. K.; Snook, B.; Herrington, R.; Fairhurst, R. J., Miner. Eng. **2009**, 22, 1119-1129.

[22] Hata, Y.; Purwanto, H.; Hosokai, S.; Hayashi, J.; Kashiwaya, Y.; Akiyama, T., Energy & Fuels **2009**, 23, 1128-1131.

[23] Hosokai, S.; Matsui, K.; Okinaka, N.; Ohno, K.; Shimizu, M.; Akiyama, T., Energy & Fuels **2012**, 26, 7274-7279.

[24] Sing, K.S.W.; Everett, D.H.; Haul, R.A.W.; Moscou, L.; Pierotti, R.A.; Rouquerol, J.; Siemieniewska, T., Pure & Appl. Chem. **1985**, 57, 603-619.

[25] Tang, J. A.; Valix, M., Miner. Eng. **2006**, 19, 1274-1279.

[26] Barroso-Quiroga, M; Castro-Luna, A, Int. J. Hydrogen Energy **2010**, 35, 6052-6056.

[27] Baudouin, D; Rodemerck, U; Krumeich, F; Mallmann, A; Szeto, K; Menard, H; Veyre, L; Candy, J-P; Webb, P; Thieuleux, C; Coperet, C, J. Catal. **2013**, 297, 27-34.

Chapter 3

Effects of Reduction on the Catalytic Performance of Ni-containing goethite Ore

3-1. Introduction

Unutilized high-temperature waste heat and CO_2 emissions are important issues in the steel industry. Significant amounts of high-temperature waste heat (> 600 °C) are emitted from blast furnaces, coke ovens, and converters without effective heat recovery [1]. The steel industry also emits large quantities of CO_2, which comprise around 15% of the total CO_2 emissions of Japan [2]. The dry reforming reaction of methane ($CH_4 + CO_2 \rightarrow 2H_2 + 2CO$; $\Delta H = 247$ kJ mol^{-1} at 298 K) is an effective method to produce energy in the form of hydrogen and carbon monoxide from carbon dioxide and waste heat [3].

The dry reforming reaction proceeds in the presence of metal based catalysts. Ni-based catalysts have been found to be one of the most effective catalysts for this reaction [4–17]. Generally, Ni-based catalysts are prepared using a wet impregnation method from Ni nitrate solution with an oxide support. To improve the catalytic performance and stability of Ni-based catalysts, many studies have

been performed. For example, alkali metals or alkaline earth metals have been added to the support materials to reduce the amount of carbon deposition and to improve catalytic stability [6–8]. Ni-containing oxides, such as perovskite and spinel compounds, exhibit strong interactions between the metal and its support [9–12]. Ni-based bimetallic catalysts have been also fabricated, and they exhibit high reactivity and stability [13–17].

In the present study, Ni-containing goethite ore was examined as a catalyst for the dry reforming reaction because of its simple preparation method, naturally occurring raw materials, low cost, and low resource utilization compared with previously reported Ni-based catalysts. Goetihte ore requires only a simple dehydration process before it can be used as a catalyst. It is mainly composed of FeOOH, which is readily decomposed to porous Fe_2O_3 by heat treatment at 300–800 °C [18,19]. Goethite ore is naturally occurring and readily available. Therefore, it is significantly less expensive than commercially available catalysts. Generally, Ni-supported catalysts lose their catalytic activities by carbon deposition and cannot be used after deactivation, but goethite ore can be recycled into iron and nickel by reduction after catalyst deactivation.

Previously, we reported that Ni-containing goethite ore was an effective catalyst for the dry reforming reaction [20]. Ni-containing goethite ore exhibited the highest catalytic activity of the three ore-based catalysts tested in the previous study (Ni-containing goethite ore, Ni-supported goethite ore, and goethite ore without Ni). In this study, the effects of hydrogen reduction on the structure and catalytic

performance of the Ni-containing goethite ore were examined in detail.

3-2. Materials and experimental methods

3-2-1. Preparation of the catalyst from goethite ore

Goethite ore (from Philippines) containing 1.18 wt% Ni, 47.98 wt% Fe, 0.14 wt% S, 2.12 wt% SiO_2, 1.26 wt% MnO, 0.47 wt% MgO, 0.10 wt% TiO_2, 3.32 wt% Cr_2O_3, 0.10 wt% Co_3O_4, and 12.6 wt% of combined water (CW) was used as a catalyst for the dry reforming reaction of methane. This goethite ore was crushed into 125–300 μm sized particles and heated to 500 °C at a heating rate of 5 °C min^{-1}; subsequently, it was calcined at this temperature for 4 h in air using a muffle furnace to remove any CW. These calcination conditions were enough for the complete dehydration of the goethite ore [20].

10 wt% Ni/Al_2O_3 catalyst as a reference was prepared by the following steps. α-Al_2O_3 reagent (35–50 μm, 99.0% up, Kanto Chemical Co., Inc., Tokyo, Japan) was added into $Ni(NO_3)_2 \cdot 6H_2O$ aqueous solution and the solution was evaporated at 80 °C. The obtained material was then calcined at 500 °C for 4 h in air.

3-2-2. Catalytic tests

The apparatus for the catalytic tests in this study was same as reported in detail elsewhere [20]. The dehydrated goethite ore was placed in a packed bed reactor consisting of a quartz tube (φ6 mm × 554 mm) and an infrared gold image furnace (RHL-E410P, ADVANCE RIKO, Inc., Yokohama, Japan). The temperature of the furnace was measured using a thermocouple placed just below the catalyst and

controlled with a temperature controller. The catalysts were placed in the quarts reactor. The amount of the goethite ore catalyst and the Ni/Al_2O_3 catalyst were 300 and 30 mg, respectively. Different amount of the catalysts was placed to set almost same Ni amount in the reactor. The length of the ore catalyst bed was around 15 mm. In all the catalytic tests, the temperature of the catalyst region was maintained at 800–900°C for 6 h. Gases were flowed into the reactor from its top side, and their flow rates were controlled using mass flow controllers. The input gases, CH_4 (> 99.9%), CO_2 (> 99.99%), and H_2 (> 99.99999%), were diluted with Ar (> 99.999%). The total flow rate of the input gases was maintained at 30 L h^{-1} $g\text{-}_{catalyst}^{-1}$. The effects of hydrogen reduction on the catalytic performance of the limonitic laterite ore were determined using three different experiments (Figure 3-1).

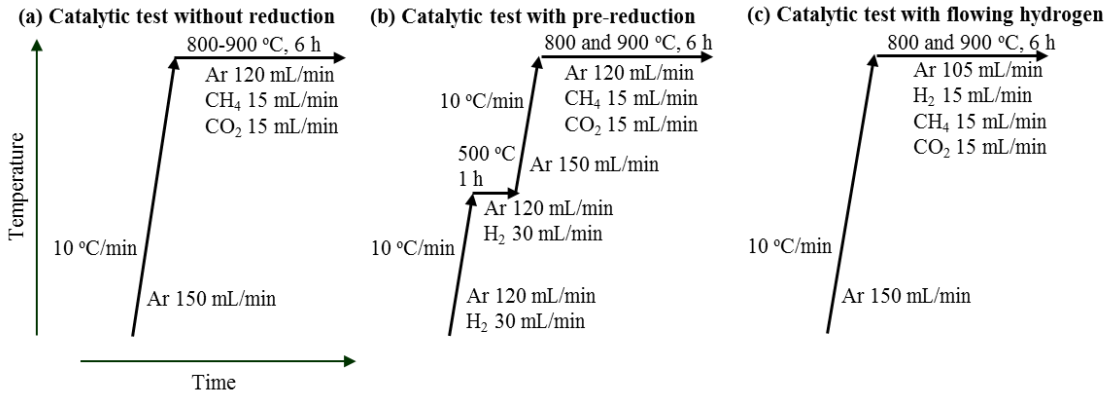

Figure 3-1 Three kinds of catalytic tests in this study.

3-2-2-1. Catalytic tests without pre-reduction (Figure 3-1, (A))

The ore catalyst was heated to 800–900 °C at a heating rate of 10 °C min^{-1} in an Ar flow of 150 mL min^{-1}. Just before the target temperature was reached, Ar (120 mL min^{-1}), CH_4 (15 mL min^{-1}) and CO_2 (15 mL min^{-1}) were flowed over the catalyst. After that, the catalyst region was maintained at these conditions for 6 h.

3-2-2-2. Catalytic tests with pre-reduction (Figure 3-1, (B))

In this experiment, the ore catalyst was reduced by hydrogen prior to the catalytic tests. The catalyst region was heated to 500 °C at a heating rate of 10 °C min^{-1} and maintained at 500 °C for 1 h while Ar (120 mL min^{-1}) and H_2 (30 mL min^{-1}) were flowed over the catalyst. After the reduction process was complete, the H_2 flow was stopped and the catalyst was heated to 800 or 900 °C at a rate of 10 °C min^{-1}. Just before the target temperature was reached, Ar (120 mL min^{-1}), CH_4 (15 mL min^{-1}), and CO_2 (15 mL min^{-1}) were flowed over the catalyst. After that, the catalyst region was maintained in this condition for 6 h.

3-2-2-3. Catalytic tests with hydrogen flow (Figure 3-1, (C))

The ore catalyst was heated to 800–900 °C at a heating rate of 10 °C min^{-1} in an Ar flow (150 mL min^{-1}). Just before the target temperature was reached, Ar (105 mL min^{-1}), H_2 (15 mL min^{-1}), CH_4 (15 mL min^{-1}), and CO_2 (15 mL min^{-1}) were flowed over the catalyst. After that, the catalyst region was maintained in this

condition for 6 h.

3-2-3. Characterization

In each catalytic test, the composition of the outflow gases was determined at 5 min interval using gas chromatography (Agilent 3000, INFICON Co., Ltd., Yokohama, Japan). Before and after the catalytic tests, phase identification and surface observation measurements of the ore were conducted using X-ray diffractometry（XRD; Miniflex, Rigaku, Tokyo, Japan) and scanning electron microscopy (SEM; JSM-7001FA, JEOL, Tokyo, Japan) with energy dispersive X-ray spectroscopy (EDS). The specific surface area of the ore was evaluated by N_2 gas adsorption measurements (Autosorb 6AG, Yuasa Ionics CO. Ltd., Osaka, Japan). Carbon formation on the catalysts was observed using a CHN/O/S elemental analyzer (CE-440; EAI, United States).

3-3. Results and discussion

3-3-1. Specific surface areas of the ore catalysts

The specific surface areas of the ore catalysts were evaluated by the Brunauer-Emmett-Teller (BET) model. Table 3-1 shows the BET surface area of the ore before and after the catalytic tests.

Table 3-1. BET surface areas of the ore catalysts before and after the catalytic tests.

	Before catalytic tests		Catalytic tests without pre-reduction			Catalytic tests with pre-reduction		Catalytic tests with flowing hydrogen	
	raw ore	after DH	800°C	850°C	900°C	800°C	900°C	800°C	900°C
BET surface area (m^2/g)	79.4	101.4	14.8	4.9	2.7	7.0	2.2	9.0	2.7

The BET surface area of the ore catalyst before and after dehydration has been previously reported [20] and it was 79.4 m^2 g^{-1} before dehydration (DH) and 101.4 m^2 g^{-1} after DH at 500 °C. The ore had cracks and it already had high surface area before DH. During DH, FeOOH was transformed into Fe_2O_3 by the following DH reaction and nano-sized pores formed [20], resulting in higher BET surface area after DH.

$$2FeOOH \rightarrow Fe_2O_3 + H_2O \qquad (3\text{-}1)$$

After the catalytic tests, the nanopores disappeared due to sintering and the surface areas of the ores were significantly decreased at higher temperatures. Compared with the catalytic tests without pre-reduction, the decrease in the surface area was more significant after catalytic tests with pre-reduction and flowing hydrogen since the ore had metallic phases which were easily sintered during the catalytic tests.

3-3-2. Catalytic tests with three different conditions

Before the catalytic tests, the condition of hydrogen reduction for the goethite ore was determined. The dehydrated goethite ore was heated up to 500 °C in H_2/Ar atmosphere (30 mL min^{-1} of H_2 and 120 mL min^{-1} of Ar). After heated, the ore was maintained at this temperature for different holding times. Table 3-2 and Figure 3-2 show the weight decrease of the ore at the different holding time and XRD patterns of the ore before and after the hydrogen reduction.

The amount of weight decrease was higher at longer holding time, however, it did not change after 1 h holding. This meant 500 °C and 1 h reduction was enough for the goethite ore. XRD patterns also revealed that only iron peaks were obtained after holding of 1 h. That is why, the reduction condition of the goethite ore was determined to be at 500 °C for 1 h.

Table 3-2. The amount of weight decrease of the goethite ore during hydrogen reduction.

Holding time (min.)	Weight decrease (%)
0	9.49
15	13.9
30	17.2
60	21.3
120	23.1
240	22.8
480	22.8

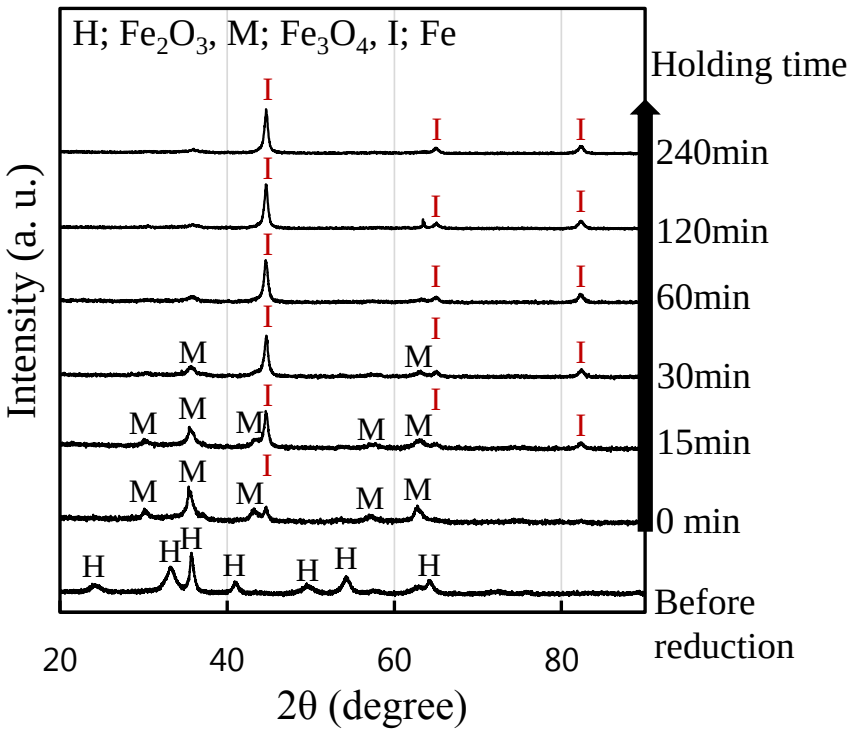

Figure 3-2. XRD patterns of the goethite ores before and after hydrogen reduction at 500 °C for different holding times.

Figures. 3-3 and 3-4 show the consumption rates of the input CH_4 and CO_2 gases and the H_2/CO ratio in the output gas during the catalytic test without pre-reduction (Ar: CH_4: CO_2 = 8:1:1), with pre-reduction (Ar: CH_4: CO_2 = 8:1:1), and flowing hydrogen (Ar: H_2: CH_4: CO_2 = 7:1:1:1). The consumption rate of CH_4 and CO_2 was the highest in the catalytic test with flowing hydrogen, followed by the catalytic test without reduction and the catalytic test with pre-reduction.

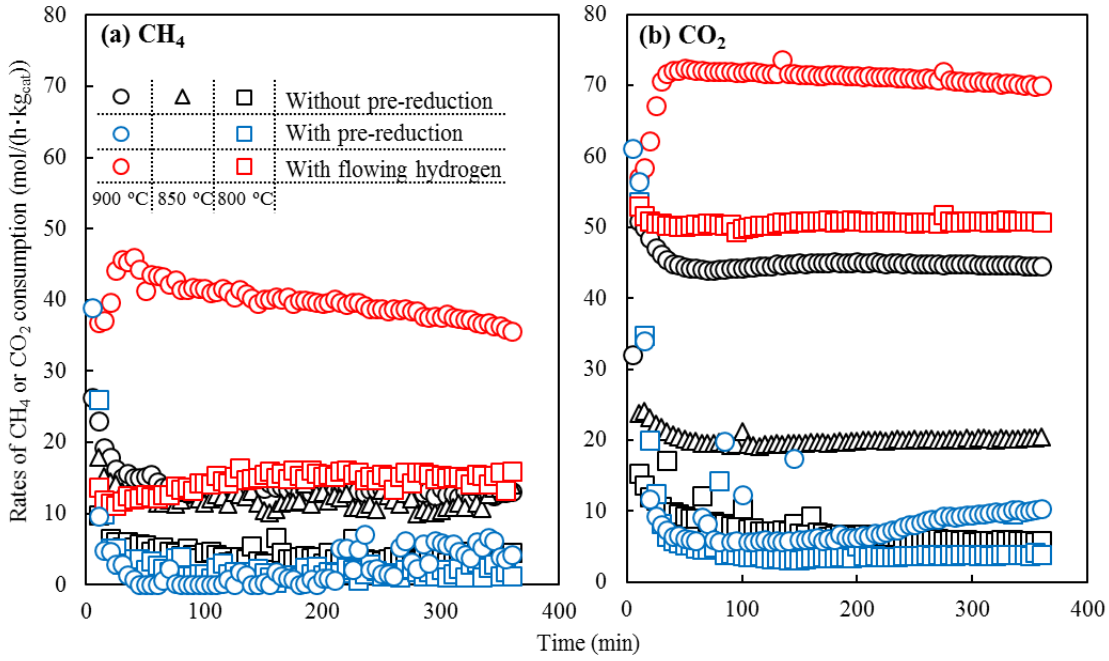

Figure 3-3 Rates of (a): CH_4 and (b): CO_2 consumption during the catalytic tests without reduction (black, Ar:CH_4:CO_2 = 8:1:1), the catalytic test with pre-reduction (blue, Ar:CH_4:CO_2 = 8:1:1), and the catalytic test with flowing hydrogen (red, Ar:H_2:CH_4:CO_2 = 7:1:1:1). The temperature was 800–900 °C and the gas flow rate was 30 L/(h·g_{cat}).

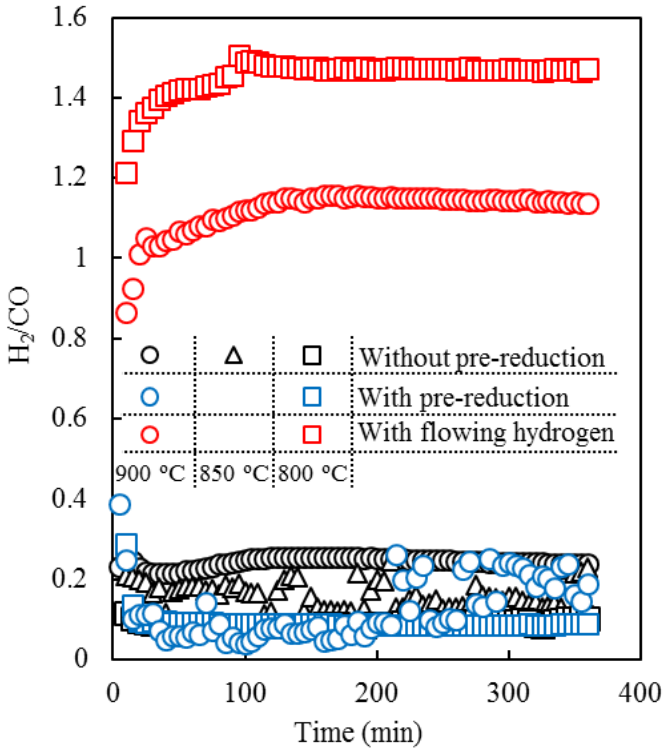

Figure 3-4. H_2/CO ratio in the output gases during the catalytic test without reduction (black, Ar:CH_4:CO_2 = 8:1:1), the catalytic test with pre-reduction (blue, Ar:CH_4:CO_2 = 8:1:1), and the catalytic test with flowing hydrogen (red, Ar:H_2:CH_4:CO_2 = 7:1:1:1). The temperature was 800–900 ºC and the gas flow rate was 30 L/(h·g_{cat}).

The difference in the catalytic performances is likely related to the state of the goethite ore catalyst. Fig. 3-5 shows the SEM-EDS images of the goethite ores after catalytic tests with pre-reduction at 800 and 900 °C, and with flowing hydrogen at 900 °C. Significant Ni segregation was observed in the goethite ore catalysts after the catalytic tests with pre-reduction at 800 and 900 °C. However, no segregation

was observed after the catalytic test with flowing hydrogen at 900 °C, despite the higher reaction temperature.

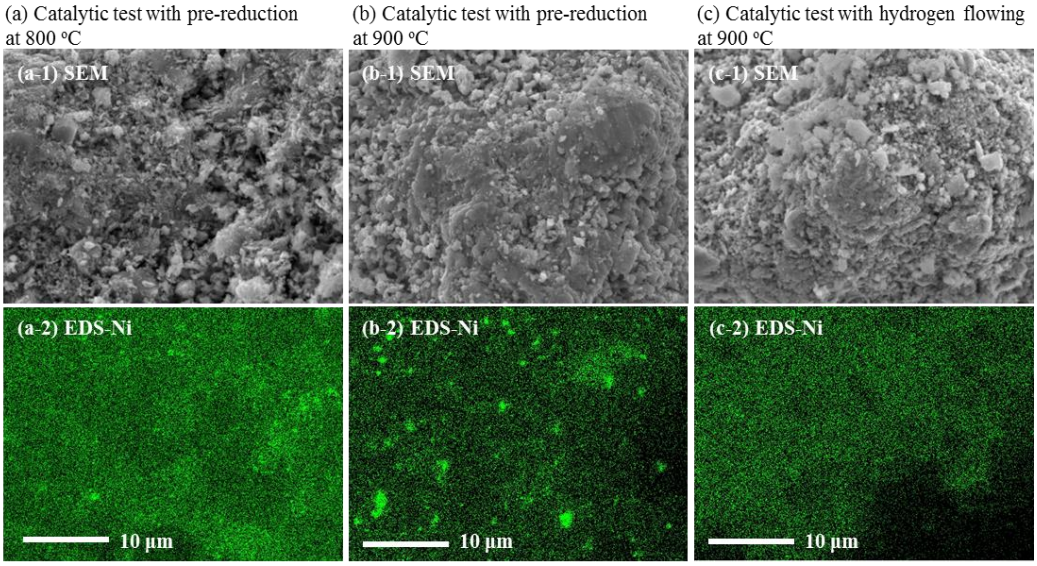

Figure 3-5. SEM (upper) and EDS (lower) images of the goethite ores after catalytic tests at 800 °C (a-1 and a-2) and 900 °C (b-1 and b-2) with pre-reduction and catalytic tests with flowing hydrogen at 900 °C (c-1 and c-2).

Figure 3-6 (A) shows XRD patterns of the ore catalysts before and after the catalytic tests and Figure 3-6 (B) shows the detailed XRD patterns of the catalysts after the catalytic tests with flowing hydrogen at $2\theta = 44–45°$. The bottom two lines in Figure 3-6 (A) represent the goethite ore before and after DH. It was confirmed that the dehydration reaction ($2FeOOH \rightarrow Fe_2O_3 + H_2O$) occurred completely after DH at 500 °C for 4 h.

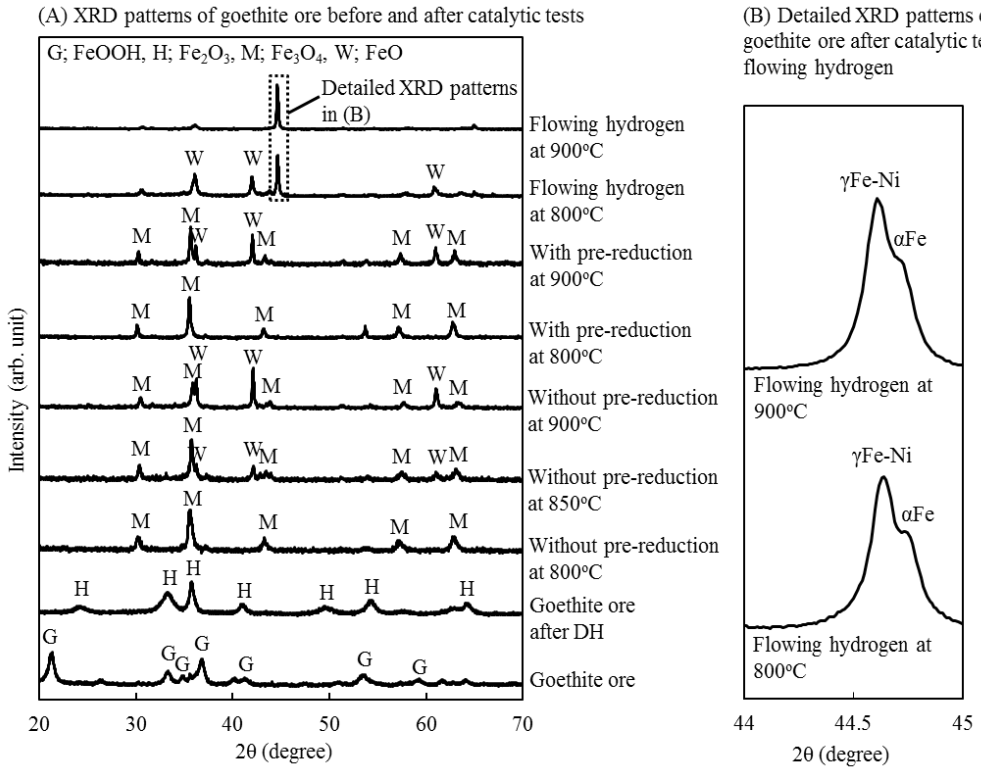

Figure 3-6 (A) XRD patterns of goethite ore, after DH, after the catalytic test at 800-900 °C without reduction ($Ar:CH_4:CO_2$ = 8:1:1), after the catalytic test at 800 and 900 °C with pre-reduction ($Ar:CH_4:CO_2$ = 8:1:1), and after the catalytic test at 800 and 900 °C with flowing hydrogen ($Ar:H_2:CH_4:CO_2$ = 7:1:1:1). (B) Detailed XRD patterns of goethite ore after the catalytic test at 800 and 900 °C with flowing hydrogen ($Ar:H_2:CH_4:CO_2$ = 7:1:1:1). The total gas flow rate to the ore catalyst was 30 $L/(h \cdot g_{cat})$.

The other XRD patterns represent the goethite ore after the catalytic tests where Fe_3O_4 or FeO were dominant after the catalytic test without and with pre-reduction. Two separated peaks corresponding to Fe and Fe-Ni were observed at around $2\theta = 44.6°$ in Figure 3-6 (B). This can be explained by the Fe-Ni phase diagram produced by Cacciamani, et al. [21,22]. Fe and Ni comprise 48.0 and 1.2 wt% of the goethite ore, respectively, meaning the average mole fraction of Ni was 0.024 in the ore. At this mole fraction, it is reasonable that the two separated peaks are visible. During the catalytic tests, iron and nickel oxides were reduced to metallic iron and nickel by the input H_2 and formed bimetallic Fe-Ni. These Fe and Fe-Ni components worked better as a catalyst in the dry reforming reaction.

In the case of the catalytic tests with pre-reduction, the consumption rates were comparative to the other tests only at the beginning and then suddenly decreased as the catalytic test proceeded. Catalytic performance can generally be improved by pre-reduction, but the pre-reduction condition in this study did not improve the performance of the ore catalyst. This is likely related to re-oxidation during the catalytic test. Fig. 3-7 shows the XRD patterns of the ore catalysts after the catalytic tests with pre-reduction. The catalytic tests were performed at 900 °C for 15, 60, and 360 min. The bottom XRD pattern shows ore catalyst after the pre-reduction, and just before the catalytic test. The catalyst reduction to Fe and Fe-Ni after pre-reduction was confirmed, however, it was re-oxidized to Fe_3O_4 and FeO even after 15 min of the catalytic test. The Fe-Ni phase was lost by this re-oxidation and the catalytic performance of the goethite ore was significantly decreased. After that, the catalyst was additionally oxidized to a single phase of Fe_3O_4 at 60 min, then

partially reduced to FeO at 360 min. The change in the catalytic performance around the 200-min mark (Fig. 3-3) may arise from the transformation of Fe_3O_4 to FeO. This would indicate that the catalytic performance of FeO is better than Fe_3O_4.

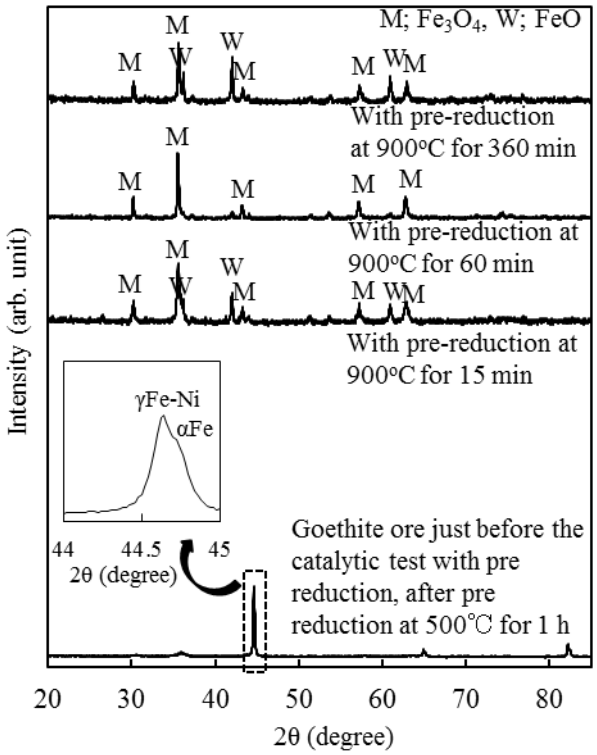

Figure 3-7. XRD patterns of goethite ore after the catalytic test with pre-reduction ($Ar:CH_4:CO_2$ = 8:1:1) at 900 °C for 15, 60, 360 min.

The consumption rates were always higher for the CO_2 than for CH_4. The H_2/CO ratios in the catalytic tests without and with pre-reduction were much lower than the one-to-one ratio theoretically expected (Fig. 3-4). This is because the product H_2 from the dry reforming reacted with the input CO_2 gas to produce CO and H_2O via the following reaction.

$$H_2 + CO_2 \leftrightarrow CO + H_2O \qquad (3\text{-}2)$$

H_2/CO ratio was the highest in the catalytic test flowing hydrogen, followed by the catalytic test without reduction and the catalytic test with pre-reduction. 10 vol% of H_2 was flowed during catalytic test with flowing hydrogen, that is why, the H_2/CO was much higher in the catalytic test with flowing hydrogen. The H_2/CO ratio was higher at high temperatures.

In this study, no carbon deposition was detected on the surface of the goethite ore after the catalytic tests. Carbon formation was less than 0.3 wt% in all of the experimental conditions.

3-3-3. Comparison of the Ni-containing goethite ore and Ni/Al_2O_3 catalysts

Fig. 3-8 (A) shows the CH_4 consumption rates on the goethite ore catalyst and the 10 wt% Ni/Al_2O_3 catalyst. The obtained consumption rates were normalized by the Ni amount in these catalysts. Conventional Ni/Al_2O_3 catalyst showed higher catalytic performance than the ore catalyst. The catalytic performance in the dry reforming reaction depends strongly on its support and Al_2O_3 is comparatively good among oxide supports for Ni [23,24]. Takano et al. reported that the dry reforming reaction mainly occurs at the interface between metal and its support [25]. The goethite ore contains small amount (2.12 wt% SiO_2, 1.26 wt% MnO, 0.47 wt% MgO, 0.10 wt% TiO_2, 3.32 wt% Cr_2O_3) of stable oxides. Among these oxides, for example, SiO_2 and TiO_2 are poorer supports for Ni-based catalysts compared with Al_2O_3 support [24]. That is why, there was less effect of support in the ore catalyst, resulting in lower catalytic performance than that of the Ni/Al_2O_3 catalyst. However, the catalytic stability was better in the goethite ore. The catalytic performance continued to drop in the Ni/Al_2O_3 and 10% decrease in the CH_4 consumption rate was observed after 6 h experiment. On the other hand, although the goethite ore showed less performance, it was more stable during catalytic use.

In addition, the goethite ore should be much superior in terms of cost to produce the catalyst. We conducted cost benefit analysis for the catalysts and the results were shown in Fig. 3-8 (B). Cost benefit performance (CBP), which were used for this analysis, was defined by the following equation;

CBP = (Performance of the catalyst)/(Catalyst production cost)

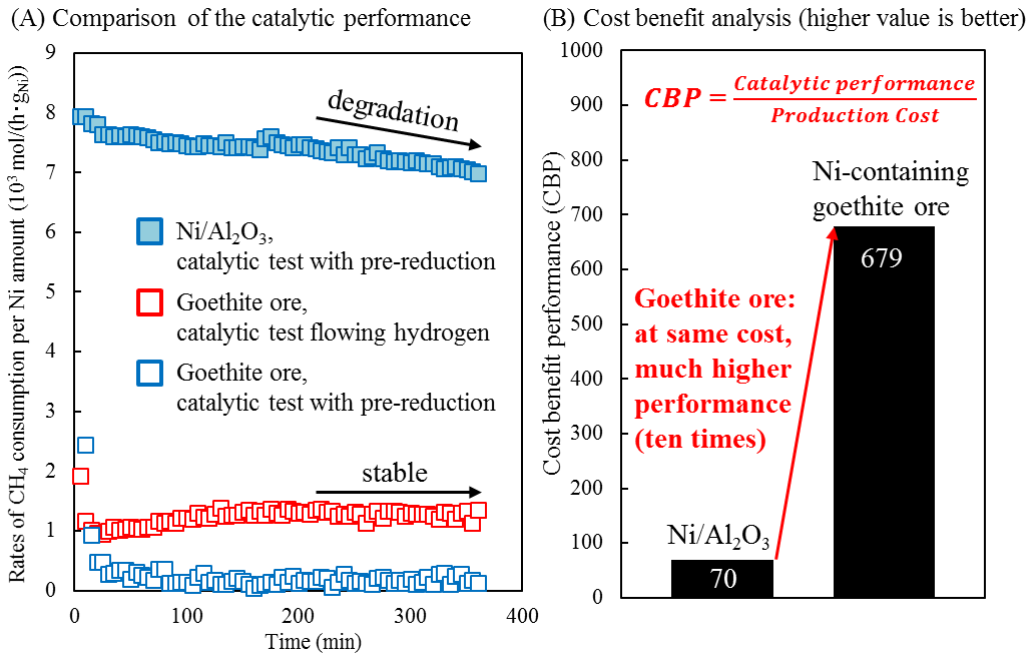

Figure 3-9. (A) Rates of CH_4 consumption (normalized by the Ni amount in the catalysts) on the Ni/Al_2O_3 and goethite ore catalysts during the catalytic tests with pre-reduction ($Ar:CH_4:CO_2$ = 8:1:1) and the catalytic test with flowing hydrogen ($Ar:H_2:CH_4:CO_2$ = 7:1:1:1) at 800 ℃. (B) Cost benefit analysis for the goethite ore and the Ni/Al_2O_3. Cost benefit performance (CBP) (= Performance of the catalyst (CH_4 consumption rate)/Catalyst production cost) was used to conduct the analysis.

In this study, the performance of the catalyst meant the rate of CH_4 consumption (mol h^{-1} $kg_{catalyst}^{-1}$). The costs of the goethite ore (1.5 wt%Ni) and industrial catalysts without rare metal are said to be 0.023-0.024 $/kg [26] and 100 $/kg [27]. These prices were used for the analysis. From the definition, higher CBP means it

is better catalyst. The goethite ore showed ten times larger CBP as the Ni/Al_2O_3. The goethite ore was much better catalyst taking into account the production cost.

3-4. Summary

In this study, the catalytic activity of Ni-containing goethite ore in the dry reforming reaction ($CH_4 + CO_2 \rightarrow 2H_2 + 2CO$) was evaluated in three types of catalytic tests; catalytic tests without pre-reduction, with pre-reduction, and with flowing hydrogen.

During dehydration process at 500 ℃, FeOOH in the goethite ore perfectly transformed into Fe_2O_3 and the surface area of the ore got higher because nanopores were introduced in the ore. The surface area drastically decreased after the catalytic tests because the nanopores were eliminated more at higher temperatures due to sintering.

The three kinds of catalytic tests revealed that the catalytic performance of the goethite ore depended on the iron phase. In this study, the phase of iron in the goethite ore changed to oxides (Fe_3O_4 and FeO) and metals (Fe and Fe-Ni). When the iron mainly existed as oxides, the catalytic performance of the FeO was better than that of Fe_3O_4. Fe and Fe-Ni showed much greater catalytic performance than the oxides.

The catalytic performance which was normalized by the Ni content of the Ni supported Al_2O_3 catalyst was better than that of the Ni-containing goethite ore catalyst due to the effect of catalyst support, however, the ore catalyst was more stable during catalytic use and much cheaper than the Ni/Al_2O_3.

REFERENCES

[1] T. Akiyama, J. Yagi, Tetsu to Hagane 82 (1996) 177–184 (in Japanese).

[2] D. Gielen, Y. Moriguchi, Energy Policy 30 (2002) 849–863.

[3] T. Akiyama, K. Oikawa, T. Shimada, E. Kasai, J. Yagi, ISIJ Int. 40 (2000) 288–291.

[4] S. Wang, G.Q.M. Lu, Appl. Catal., B 16 (1998) 269–277.

[5] J. A. Montoya, E. Romero-Pascual, C. Gimon, P. Del Angel, A. Monzon, Catal. Today 63 (2000) 71–85.

[6] M. Barroso-Quiroga, A. Castro-Luna, Int. J. Hydrogen Energy 35 (2010) 6052–6056.

[7] T. Horiuchi, K. Sakuma, T, Fukui, Y. Kubo, T. Osaki, T. Mori, Appl. Catal., A 144 (1996) 111–120.

[8] Z. Alipour, M. Rezaei, F. Meshkani, J. Ind. Eng. Chem. 20 (2014) 2858–2863.

[9] G. Gallego, C. Batiot-Dupeyrat, J. Barrault, E. Florez, F. Mondragon, Appl. Catal., A 334 (2008) 251–258.

[10] K. Sutthiumporn, T. Maneerung, Y. Kathiraser, S. Kawi, Int. J. Hydrogen Energy 37 (2012) 11195–11207.

[11] L. Zhou, L. Li, N. Wei, J. Li, J. Basset, ChemCatChem 7 (2015) 2508–2516.

[12] N. Sahli, C. Petit, A.C. Roger, A. Kiennemann, S. Libs, M.M. Bettahar, Catal. Today 113 (2006) 187–193.

[13] S. Theofanidis, V. Galvita, H. Poelman, G. Marin, ACS Catal. 5 (2015) 3028–3039.

[14] K. Ray, S. Sengupta, G. Deo, Fuel Process. Technol. 156 (2017) 195–203.

[15] J. Zhang, H. Wang, A. Dalai, J. Catal. 249 (2007) 300–310.

[16] S. Theofanidis, R. Batchu, V. Galvita, H. Poelman, G. Marin, Appl. Catal., B 185 (2016) 42–55.

[17] Z. Huang, H. Jiang, F. He, D. Chen, G. Wei, K. Zhao, A. Zheng, Y. Feng, Z. Zhao, H. Li, J. Energy Chem. 25 (2016) 62–70.

[18] H. Naono; R J. Fujiwara, Colloid Interf. Sci. 73 (1980) 406–415.

[19] G. Saito, T. Nomura, N. Sakaguchi, T. Akiyama, ISIJ Int. 56 (2016) 1598–1605.

[20] K. Abe, G. Saito, T. Nomura, T. Akiyama, Energy Fuels 30 (2016) 8457–8462.

[21] G. Caccimani, A. Dinsdale, M. Palumbo, A. Pasturel, Intermet. 18 (2010) 1148–1162.

[22] G. Caccimani, J. De Keyzer, R. Ferro, U.E. Klotz, J. Lacaze, P. Wollants, Intermet. 14 (2006) 1312–1325.

[23] A. Takano, T. Tagawa, S. Goto, J. Chem. Eng. Japan 27 (1994) 727–731.

[24] H.M. Swaan, V.C.H. Kroll, G.A. Martin, C. Mirodatos, Catal. Today 21 (1994) 571–578.

[25] A. Takano, T. Tagawa, S. Goto, Kagaku Kougaku Ronbunsyu 21 (1995) 1154–1160 (in Japanese).

[26] Base Metals News, https://www.fastmarkets.com/base-metals-news/asia/2016-review-china-imports-philippine-laterite-ore-hit-year-denr-audit-125904/ (accessed 14 September 2017).

[27] M. Iwamoto, M. Akita, M. Onaka, T. Tanaka, T. Deguchi, K. Tomishige, H. Yamashita, I. Yamanaka (2011) “How to Prepare Heterogeneous and Homogeneous Catalysts”, NTS Inc., ISBN 978-4-86043-377-2 (in Japanese).

Chapter 4

Carbon Combustion Synthesis Ironmaking from Carbon-Infiltrated Goethite Ore

4-1. Introduction

Carbon infiltrated goethite ore has been produced via chemical vapor infiltration (CVI) method using tar vapor from coal or biomass [1-8]. Reduction of the carbon infiltrated goethite ore occurs at comparatively low temperature because (1) the deposited carbon is reactive amorphous carbon and (2) close contact between the goethite ore and the deposited carbon is reachable through the nanopores of the goethite ore [7, 8]. There are two kinds of reduction reductions of iron oxide (hematite) by carbon; direct reduction and indirect reduction reactions

Direct reduction: $Fe_2O_3 + 3C \rightarrow 2Fe + 3CO$, $\Delta H_{298\,K} = 491$ kJ/mol (4-1)

Indirect reduction: $Fe_2O_3 + 3CO \rightarrow 2Fe + 3CO_2$, $\Delta H_{298\,K} = -26$ kJ/mol (4-2)

Hosokai, et al. revealed that the direct reduction reaction is dominant in the reduction of the carbon infiltrated goethite ore [8]. Taking the reduction reaction

into account, 18.4wt% of carbon is needed for perfect reduction of Fe_2O_3 to metallic iron. This direct reduction reaction is big endothermic reaction and heat source is needed to complete the reaction. When carbon amount in the carbon infiltrated ore exceeds this value, combustion of the excess carbon can be utilized as heat source for the reduction reactions. When the exothermic heat from the carbon combustion is dominant, the total reaction (carbon combustion + iron oxide reduction) can self-propagate. This is a concept of "combustion synthesis".

Combustion synthesis is an energy and time saving process and a lot of materials such as hydride [9, 10], oxides [11-13], nitrides [14, 15], and alloys [16-19] have been produced via this method. The probability of the combustion synthesis reaction can be evaluated by its adiabatic flame temperature. The adiabatic flame temperature is a maximum reachable temperature under the assumption of adiabatic system. Experientially, the combustion wave can self-propagates when the adiabatic flame temperature reaches 1800 K [20]. The adiabatic flame temperature (T_{ad}) of a combustion synthesis reaction can be calculated by the following equation [20]:

$$-\Delta H = \int_{298}^{T_{ad}} C_p dT + \Sigma \Delta H_t \qquad (4\text{-}3)$$

where ΔH is the standard enthalpy change of the reaction (J mol^{-1}), the specific heat capacity of a product is C_p (J mol^{-1} K^{-1}), and ΔHt is the enthalpy change of transformation (J mol^{-1}).

Carbon-infiltrated goethite ore produced via the CVI method is favorable for direct ironmaking; reduction of the ore proceeds at lower temperature because the

deposited carbon and the ore wall have very close contact and the deposited carbon is a highly reactive amorphous carbon. However, the amount of the deposited carbon in the goethite ore through the CVI process is only around 5 mass%, meaning that perfect reduction to iron is unable using the ore. In addition to CVI, preparation of carbon-infiltrated iron ore using various iron sources and tar has been investigated [21-23]. High carbon contents of up to 50 mass% in goethite ore are attainable using an impregnation method in which the ore and tar are directly mixed and heated [23]. Although such an attractive raw material can be produced from mildly-calcined nanoporous goethite ore, the goethite ore in the actual ironmaking process is heated with coke breeze and binder at temperatures greater than 1400 °C for 20 h to satisfy the demand of the BF, which destroys the nanoporous structure of the goethite ore.

In this study, theoretical calculations were taken place for the combustion synthesis ironmaking method using carbon infiltrated iron oxide from the view point of the adiabatic flame temperature. The initial composition of the iron oxides and the amount of carbon infiltrated in the iron oxides were changed, and at each condition the adiabatic flame temperature was calculated. Then, carbon-infiltrated iron ores were experimentally produced from coal tar-based liquid and select iron sources including nanoporous goethite ore. CS experiments were then conducted to reduce the carbon-infiltrated iron ores and the reaction mechanism was discussed in terms of the obtained results.

4-2. Calculation and experimental methods

4-2-1. Adiabatic flame temperature calculations

Thermal calculation was taken place to calculate the adiabatic flame temperature of the combustion synthesis ironmaking using a numerical software. Initial state of the iron oxide and carbon amount in the iron oxide were changed. The adiabatic flame temperature calculation was taken place at every x and y value under the following conditions and assumptions:

1) Initial carbon infiltrated iron oxide had one molar FeO_x (x = 0-1.5) and y molar carbon (y > 1).
2) Calculation was taken place at the step size of 0.02 from 0 until 1.5 for x and at the step size of 0.02 from 1 until 4 for y.
3) Starting iron oxides were only monophase or biphase; Fe/FeO at $0 < x < 1.5$, Fe_3O_4/FeO at $1 < x < 1.33$, and Fe_3O_4/Fe_2O_3 at $1.33 < x < 1.5$. All the iron oxide was perfectly reduced to metallic iron. Carbon was completely consumed during the reaction.
4) Only perfect carbon combustion reaction ($C + O_2 \rightarrow CO_2$) and direct reduction reaction ($FeO_x + C \rightarrow Fe + CO$) were considered because these reactions are dominant thermodynamically at high temperature as shown in Figure 4-1.

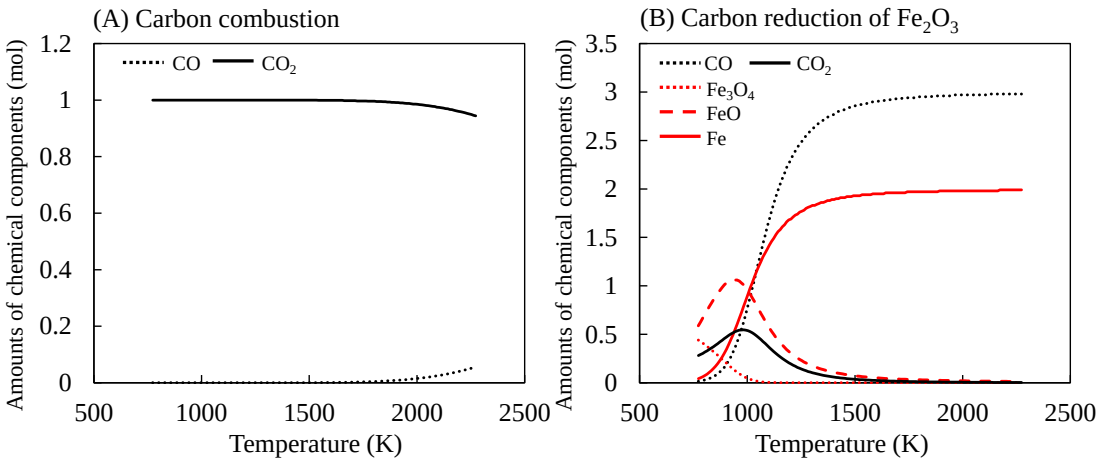

Figure 4-1. Equilibrium calculations for (A) carbon combustion reaction and (B) reduction reaction of Fe_2O_3 by carbon at different temperatures. 1mol of C and 1mol of O_2 were considered as starting materials for (A), and 1mol of Fe_2O_3 and 3mol of C for (B), respectively.

5) The enthalpy change of transformation was not taken into account.

6) The considered reaction equations and their standard enthalpy changes were as follows:

$$C + O_2 \rightarrow CO_2 \qquad (\Delta H = -394.36 \text{ kJ mol}^{-1}) \qquad (4\text{-}4)$$

$$Fe_2O_3 + 3C \rightarrow 2Fe + 3CO \qquad (\Delta H = 329.51 \text{ kJ mol}^{-1}) \qquad (4\text{-}5)$$

$$Fe_3O_4 + 4C \rightarrow 3Fe + 4CO \qquad (\Delta H = 466.51 \text{ kJ mol}^{-1}) \qquad (4\text{-}6)$$

$$FeO + C \rightarrow Fe + CO \qquad (\Delta H = 108.55\ kJ\ mol^{-1}) \qquad (4\text{-}7)$$

7) The specific heat, C_p, of a material is expressed as the following function of temperature T:

$$Cp = a + bT + cT^{-2} + dT^{2} \qquad (4\text{-}8)$$

The thermodynamic data (a, b, c, and d values) for the specific heat of the products (Fe, CO, and CO_2) [24-28] are shown in Table 4-1.

Table 4-1. Specific heat ($Cp = a + bT + cT^{-2} + dT^{2}$) of (A) Fe, (B) CO, and (C) CO_2 [24-28].

(A) Fe

Temperature range(K)	a	b × 10^3	c × 10^{-5}	d × 10^6
298-800	31.873	-22.333	-3.519	40.076
800-1142	930.624	-1445.326	-1077.585	676.725
1142-1184	-13469.674	15857.405	29209.382	-5241.395
1184-1667	24.717	7.463	-1.700	0.368
1667-1811	-10.634	30.936	275.166	-3.791
1811-	46.000	0.000	0.000	0.000

(B) CO

Temperature range(K)	a	b × 10^3	c × 10^{-5}	d × 10^6
298-800	25.867	6.508	1.105	1.020
800-2200	29.932	5.415	-10.813	-1.054
2200-	37.178	0.203	-54.490	0.004

(C) CO_2

Temperature range(K)	a	b × 10^3	c × 10^{-5}	d × 10^6
298-900	29.314	39.970	-2.484	-14.783
900-2700	54.435	5.116	-43.578	-0.806
2700-7600	76.000	-5.214	350.714	0.640

4-2-2. Preparation of carbon infiltrated ores

Figure 4-2 shows the experimental procedures including sample preparation and combustion synthesis experiments. Three raw materials (goethite ore, high-grade iron (hematite) ore, and Fe_2O_3 reagent) were used in this study. The goethite ore and high-grade iron ore contain 57 and 65 mass% of total Fe and 8.8 and 0.77 mass% of combined water (CW), respectively. The Fe_2O_3 reagent, which was used as a reference, had sizes of 2–5 mm and a purity of 99.5%. Initially, all the raw materials were crushed into 1–2 mm fragments and then calcined at 300 °C for 24 h in an air atmosphere to remove CW. Coal tar was used as the carbon source. The viscosity of tar itself is too high to infiltrate the pores of goethite ore. For this reason, toluene (C_7H_8, 99.5%) was added to the tar to reduce its viscosity. Tar and toluene were weighed at a mass ratio of 1:1 and then stirred at 50 °C to give a tar solution. 30 mL of this tar solution was placed into an alumina crucible and 10 g of the calcined iron ores were added. The iron ores with the tar solution were then heated at 500 °C for 1 h under an Ar flow. The obtained carbon-infiltrated ores were then crushed into 1–2 mm fragments.

4-2-3. Combustion synthesis (CS) experiments

CS experiments were conducted in a packed bed reactor. Carbon-infiltrated ores (100 mg) were placed into a quarts tube (φ6 mm) and a thermocouple was placed under the ore, with the ore-temperature controlled by a temperature controller. The ore was heated rapidly to the target temperature at a rate of 20 °C s^{-1} and was

maintained at that temperature for 10 s. Gases were flowed from the top to the reactor at a constant gas flow rate of 1 L min^{-1} (linear velocity: 0.6 m s^{-1}). The compositions of the flowed gases were 25 vol% O_2/Ar, Ar, or 20 vol% H_2/Ar. When O_2/Ar and H_2/Ar were flowed, the gas flow was immediately changed to Ar after the temperature was held for 10 s. Temperature changes of the samples during the CS experiments were measured every 200 ms by a thermocouple placed directly over the ore. Gas analysis was performed during the CS experiments every 1 s using gas chromatography-mass spectrometry (GC-MS, Thermostar D-35614 GSD 300 T3 Gas Analyzer Spectrometer, Pfeiffer Vacuum, Aslar, Germany). Phase identification and cross-sectional observation of the ore samples were conducted using X-ray diffractometry (XRD; Miniflex, Rigaku, Tokyo, Japan) and scanning electron microscopy (SEM; JSM-7001FA, JEOL, Tokyo, Japan) with energy dispersive X-ray spectroscopy (EDS). The amount of carbon in the ore was determined using a CHN/O/S elemental analyzer (CE-440; EAI, USA). The pore distribution, pore volume, and BET surface area were determined by N_2 adsorption–desorption measurements (Autosorb 6AG, Yuasa Ionics CO. Ltd., Osaka, Japan) at 77 K.

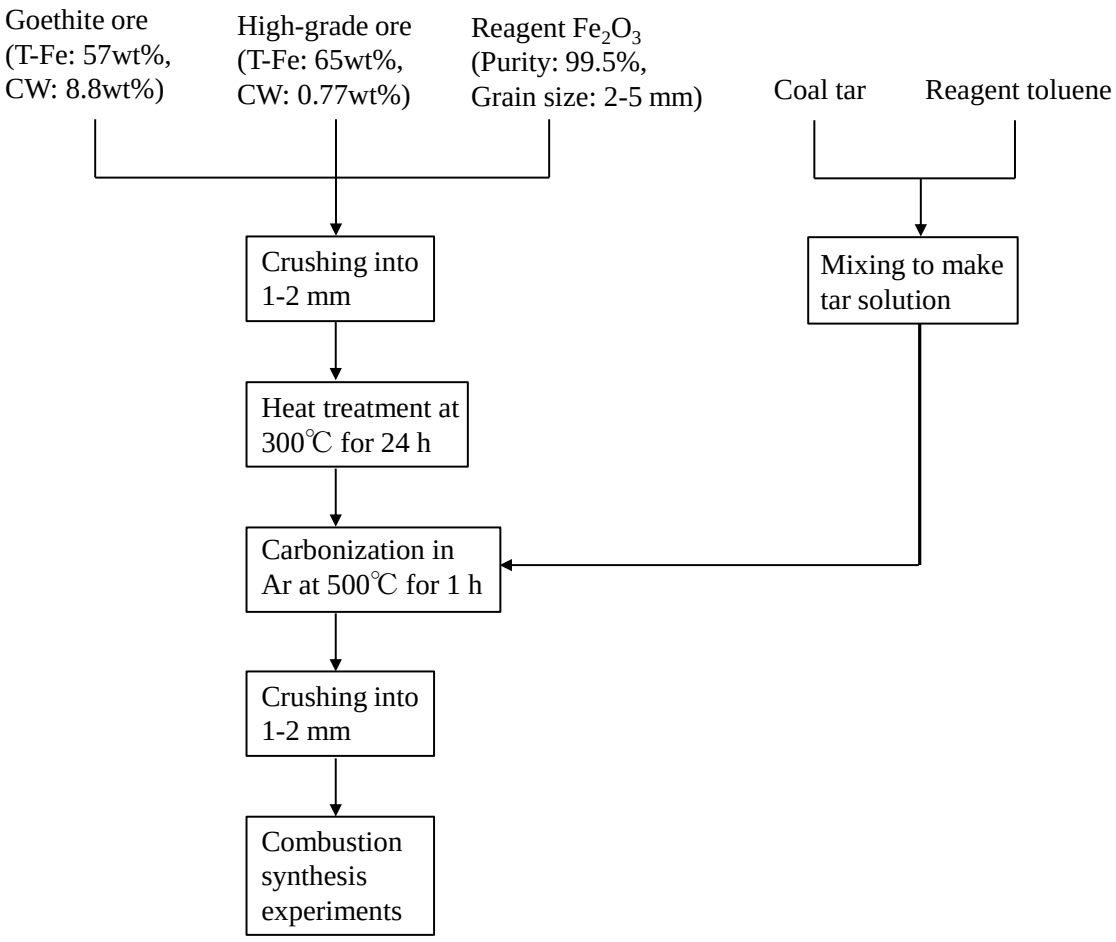

Figure 4-2. Experimental procedures in this study.

4-3. Results and discussion

4-3-1. Adiabatic flame temperature calculations

The reduction reaction of iron oxides and the carbon combustion reaction were expressed in the following eq. (4-9) and (4-10).

$$FeO_x + xC \rightarrow Fe + xCO \quad (4\text{-}9)$$

$$(y\text{-}x)C + (y\text{-}x)O_2 \rightarrow (y\text{-}x)CO_2 \quad (4\text{-}10)$$

Thus, the total reaction considered in this study was:

$$FeO_x + yC + (y\text{-}x)O_2 \rightarrow Fe + xCO + (y\text{-}x)CO_2 \quad (4\text{-}11)$$

The adiabatic flame temperature can be calculated for the eq. (4-11) by the following equation.

$$-\Delta H(\text{eq. } (4-11)) = \int_{298}^{T_{ad}} \left\{ (C_p(Fe) + xC_p(CO) + (y-x)C_p(CO_2) \right\} dT \quad (4\text{-}12)$$

Firstly, calculation of the adiabatic flame temperature was taken place for iron oxide single phases (Fe_2O_3 (x = 1.50), Fe_3O_4 (x = 1.34), and FeO (x = 1.00)). Figure 4-3 shows the relationship between the adiabatic flame temperature and y values

(carbon amount). Calculation of T_{ad} was taken place at every y value. 2.70, 2.44, and 1.84 molar of carbon for Fe_2O_3, Fe_3O_4, and FeO were needed for successful self-propagation of combustion wave. The values corresponded to 28.9, 27.5, and 23.5wt% of carbon, respectively.

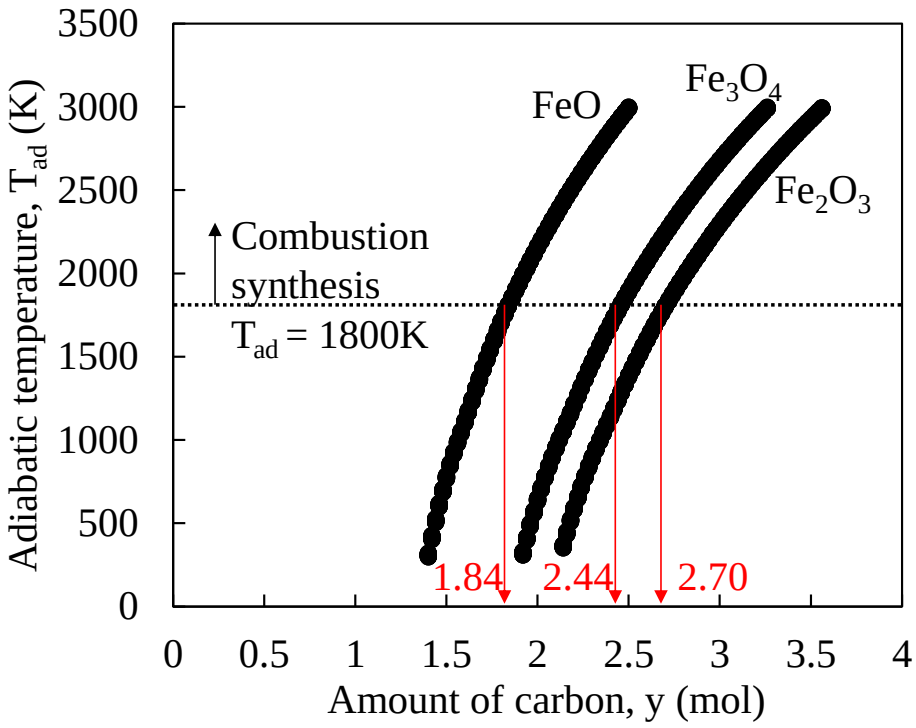

Figure 4-3 Changes of the adiabatic flame temperature T_{ad} at different x values (FeO_x) with y (carbon amount) values.

Secondly, the adiabatic flame temperature calculations were taken place for all x and y values and the results are shown in Figure 4-4. Calculations were taken

place for the composition inside the green line in Figure 4-4. The black dotted line separated endothermic and exothermic zones; at the left area of the line the reaction is endothermic, meaning combustion synthesis reaction never occurs and at the right side, exothermic. The adiabatic temperature increased in a direction toward right in this Figure; the amount of carbon increased and oxygen decreased. The increase in the amount of carbon contributed to larger exothermic heat from the carbon combustion reaction. The decrease in the amount oxygen, meaning higher reduction degree of iron oxide, contributed to lower endothermic heat in the reduction reaction.

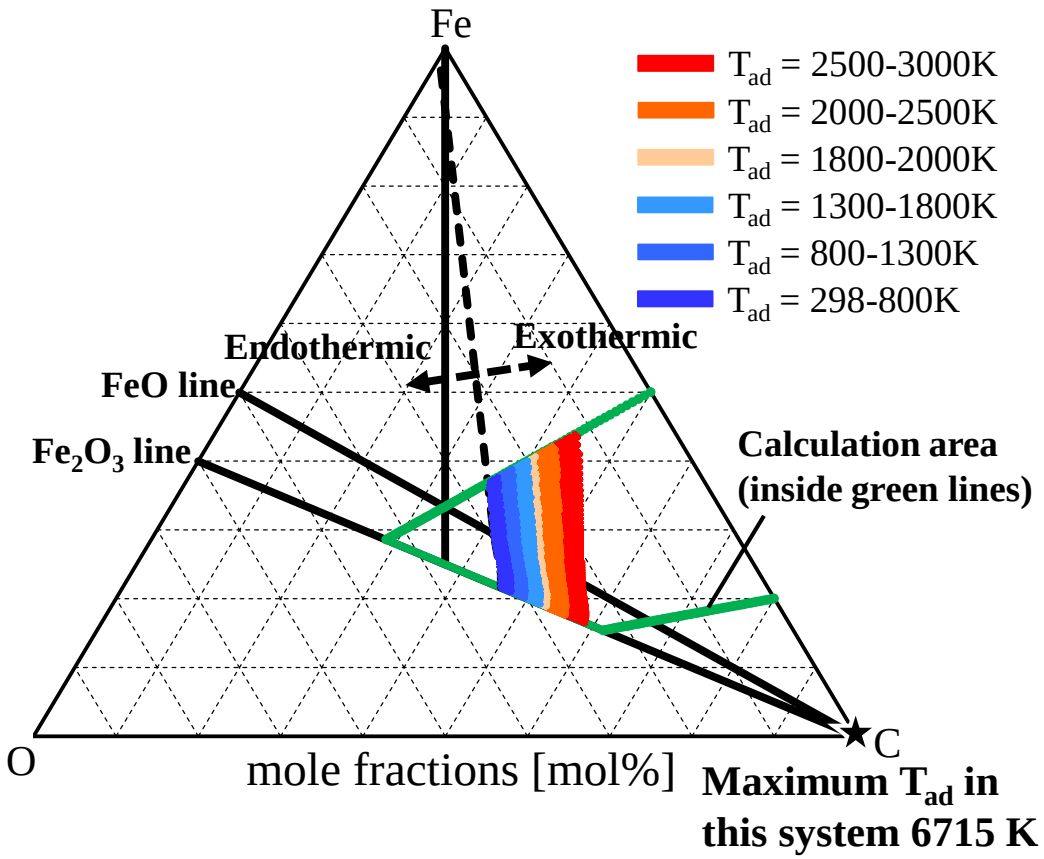

Figure 4-4 Adiabatic flame temperature calculation in a ternary diagram of Fe-O-C system.

The effects of raw materials on the carbon amount needed for successful combustion synthesis reaction were also calculated. Different kinds of carbon; graphite and amorphous carbon, and different types of iron oxide; pure iron oxide and natural iron ore, and the effect of pre-heating, were investigated.

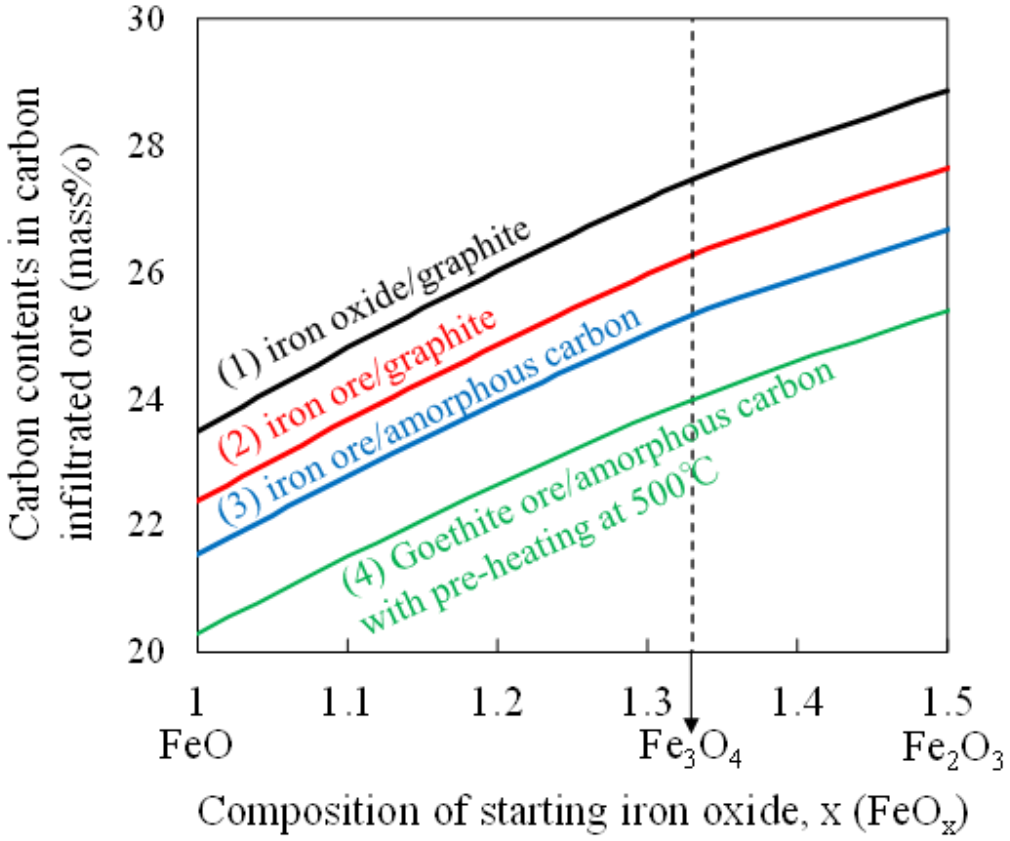

Figure 4-5 The amount of carbon in the iron oxides when the adiabatic flame temperature is 1800 K.

Table 4-2 Composition of the goethite ore before and after calcination.

	Composition (mass%)				
	T. Fe	Fe_2O_3	Al_2O_3	SiO_2	CW
Goethite ore	58.7	83.9	1.6	4.5	8.6
Goethite ore after calcination	64.3	91.9	1.8	4.9	0.0

Figure 4-5 shows the carbon amounts in the carbon infiltrated iron oxides when the adiabatic flame temperature is 1800 K. When pure iron oxides and graphite were used, 23.5—28.9mass% of C was needed for the combustion synthesis (same with Figure 4-3). Table 4-2 shows the composition of the goethite ore before and after calcination. The CW in the goethite ore was assumed to be completely removed after the calcination.

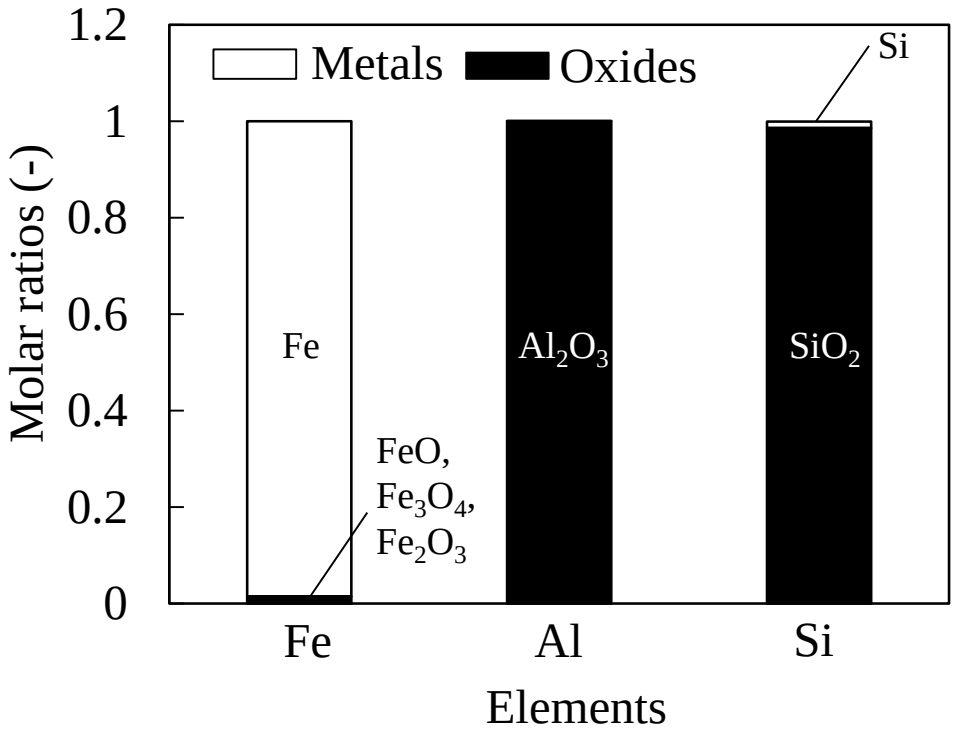

Figure 4-6 Molar ratios of metals and oxides for Fe, Al, and Si elements at the equilibrium of carbon reduction reactions at 1800K. The starting materials were 1mol of Fe_2O_3 and 3mol of C, 1mol of Al_2O_3 and 3mol of C, and 1mol of SiO_2 and 2mol of C.

The contained Al_2O_3 and SiO_2 in the natural goethite ore were assumed not to be reduced by carbon. The equilibrium compositions in the carbon reduction reactions of Fe_2O_3, Al_2O_3, and SiO_2 at 1800K are investigated in Figure 4-6. Almost of all Fe_2O_3 was reduced to metallic Fe by carbon at 1800K, however, Al_2O_3 and SiO_2 were not reduced at all. That is why the assumption that the carbon reduction of Al_2O_3 and SiO_2 did not occur was reasonable. When the calcined goethite ore was used instead of pure iron oxide, the essential carbon amount was decreased. This was because the direct reduction of iron oxide was a strong endothermic reaction. The exothermic heat from the carbon combustion reaction was used for both the endothermic reaction and temperature increase of the products. On the other hand, Al_2O_3 and SiO_2 were not reduced by carbon, so the exothermic heat was used only for temperature increase, resulting in decrease of the amount of necessary carbon for the same adiabatic flame temperature.

Cahyono et al. revealed that the deposited carbon in goethite ore by CVI method was amorphous carbon [7]. Adiabatic flame temperature calculation was taken place for the amorphous carbon infiltrated goethite ore. The amorphous carbon usage can decrease the amount of carbon in the carbon infiltrated goethite ore since the amorphous carbon was more reactive than the graphite carbon.

To produce carbon infiltrated goethite ore, calcination and carbonation processes are needed. 300—600℃ are used for the processes and the heat can be also utilized. The effect of pre-heating of 500℃ was investigated. The amount of essential carbon was able to be decreased further. 20.5—25.0mass% of carbon is

needed in the carbon (amorphous) infiltrated goethite ore with 500℃.

4-3-2. Calcination of goethite ore

Carbon-infiltrated iron ores were prepared from the goethite ore, the high-grade hematite iron ore, and the Fe_2O_3 reagent, which were pre-calcined in air. The goethite ore mainly consisted of FeOOH before calcination and completely decomposed to Fe_2O_3 via the following dehydration reaction.

$$2FeOOH \rightarrow Fe_2O_3 + H_2O \qquad (4\text{-}13)$$

For natural goethite ore, the dehydration of FeOOH begins from 230 °C, leading to the formation of ~4 mm nanopores. Although nanopores exist after calcination at 800 °C, their specific surface areas decrease drastically by calcination at higher temperatures; 230–400 °C are optimal temperatures for goethite ore calcination [29]. The goethite ore used in this study was calcined under various conditions: 300 °C for 24 h, 500 °C for 1 h, 800 °C for 1 h, 1000 °C for 24 h, and 1200 °C for 24 h. The pore size distributions, BET surface areas, and pore volumes are shown in Figure 4-7.

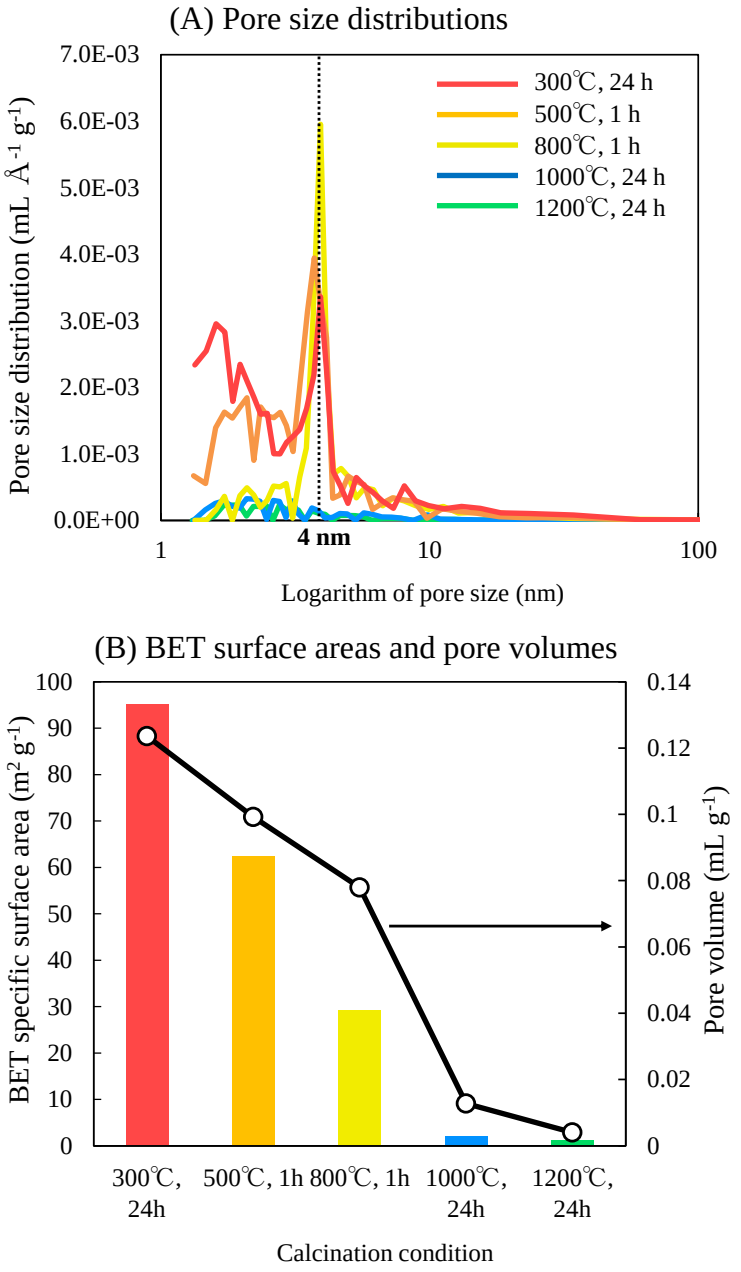

Figure 4-7 Pore distributions, BET surface areas, and pore volumes of the goethite ore after calcination at 300–1200 °C for 1 h and 24 h.

The pore size distributions were determined by the BJH method [30]. Pores smaller than ~2 nm and larger than ~4 nm were observed in the goethite ores calcined at 300 and 500 °C. According to Naono et al., two types of nanopores are existent in calcined goethite ore: larger pores (~4 nm) and smaller pores (~1 nm) [31]. The larger nanopores already exist between the primary particles in the original goethite ore, and they are comparatively stable against calcination [31]. In contrast, the smaller nanopores form during the decomposition reaction of goethite ore, and they become larger during calcination at higher temperatures [31]. The smaller pores disappeared during calcination at 800 °C, and a strong peak, corresponding to a pore size of 4 nm, was obtained. This result indicates that smaller pores grew up to ~4 nm during calcination at high temperature. Calcination at temperatures over 1000 °C completely destroyed the nanopores in the goethite ore. Thus, the goethite ore had three types of pore structures after calcination at different temperatures: i) pores ~2–4 nm (300–500 °C), ii) pores ~4 nm (800 °C), and iii) no pores (1000–1200 °C).

4-3-3. Observation of carbon infiltrated ores

For the carbon-infiltrated goethite ore, pre-calcination at 300 °C for 24 h gave rise to 24.4 mass% of C element after heat treatment with the tar solution. The ore also contained 0.64 mass% of H element, indicating that the tar solution did not completely decompose into carbon and that some of it was deposited in the form of hydrocarbons. As is shown in Figure 4-8, Fe_2O_3 in the goethite ore was partially

reduced to Fe_3O_4 after the heat treatment with the tar solution at 500 °C.

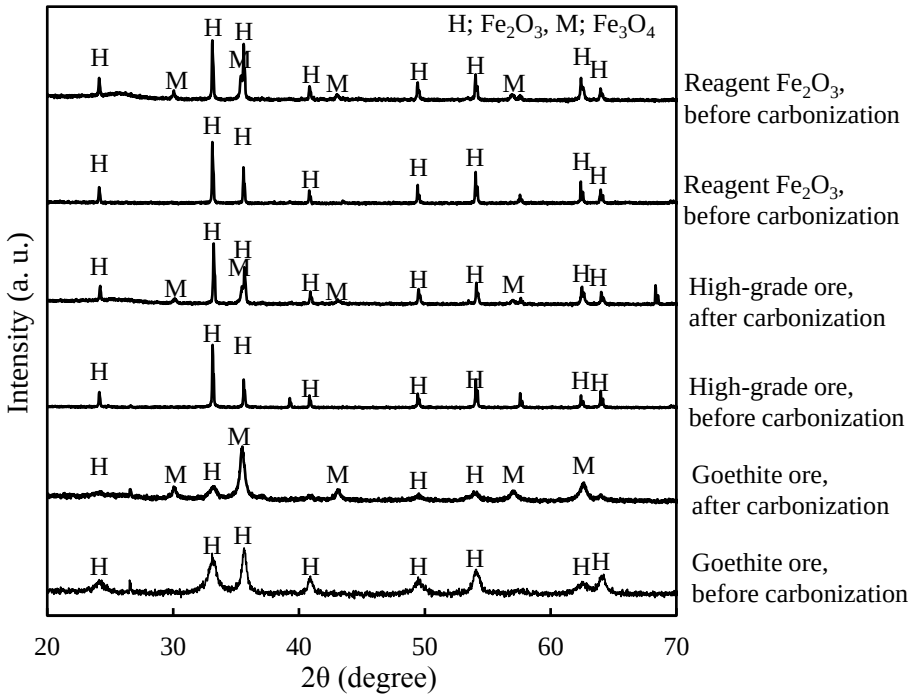

Figure 4-8 XRD patterns of the goethite ore, the high-grade hematite ore, and the reagent Fe_2O_3 before and after carbonization treatment.

Figure 4-9 shows cross-sectional SEM-EDS images of the carbon-infiltrated ores. A several hundred-micrometer thick carbon layer formed on the surface regardless of the type of raw material. However, only the goethite ore possessed a substantial amount of carbon throughout. Clearly, the tar solution successfully penetrated into the nanopores generated in the calcined goethite ore.

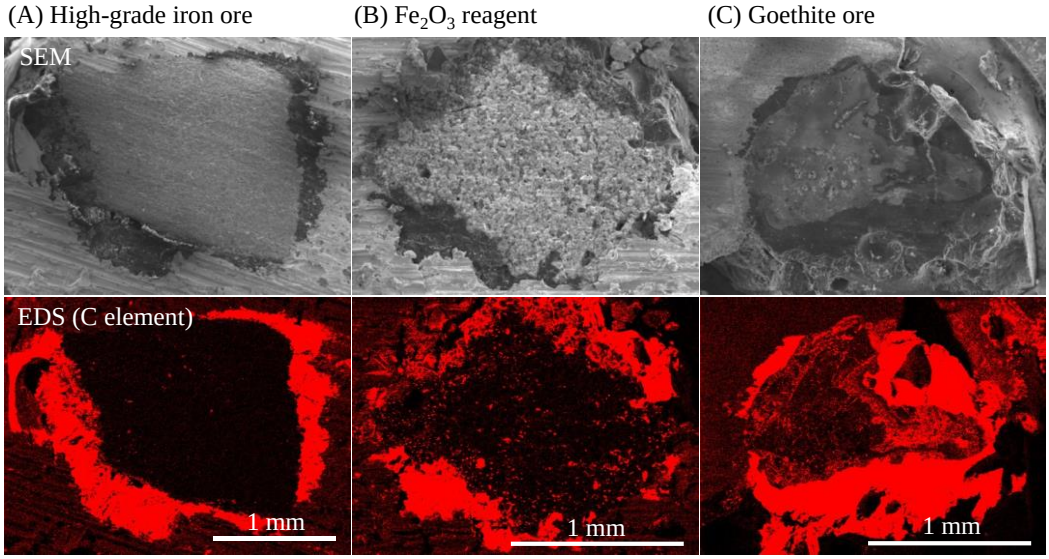

Figure 4-9. Cross-sectional SEM-EDS observations of carbon-infiltrated high-grade iron ore, Fe_2O_3 reagent, and goethite ore. The red areas in the EDS images correspond to carbon.

4-3-4. Combustion synthesis experiments

The effect of nanopores on the reduction of iron oxides was observed by using different iron sources and by changing the pre-calcination conditions. Figure 4-10 shows the XRD patterns of the products after these CS experiments. First, the effect of the type of raw material was examined. Carbon-infiltrated goethite ore, high-grade ore, and Fe_2O_3 reagent were subjected to CS conditions of 900 °C for 10 s under a 25 vol% O_2 atmosphere. These experiments confirmed that reduction proceeded to metallic iron only in the carbon-infiltrated goethite ore; only Fe_3O_4 and Fe_2O_3 were observed in the high-grade ore and the reagent (Figure 4-10A), and reduction of the iron source to metallic iron proceeded only when the goethite ore was used. The goethite ore after calcination at lower temperatures had a nanoporous structure; tar solution can easily infiltrate into the pores, resulting in contact between the goethite ore and carbon. Hosokai et al. reported that nano-order contact between iron ore and carbon is very effective for reduction [8]. They produced carbon-infiltrated iron ore from pre-calcined natural goethite ore and pyrolyzed biomass tar and reduced it under an inert atmosphere [8]. As a result, the ore was reduced at lower temperature compared with the mixture of μm-sized Fe_3O_4 reagent and carbon black or coke [8]. The carbon-infiltrated goethite ore used in this study was reduced to iron through such nano-contacts. In the case of high-grade iron ore and Fe_2O_3 reagent, however, which did not have CW, poor contact was made between the iron oxides and carbon, thereby limiting metallic iron formation.

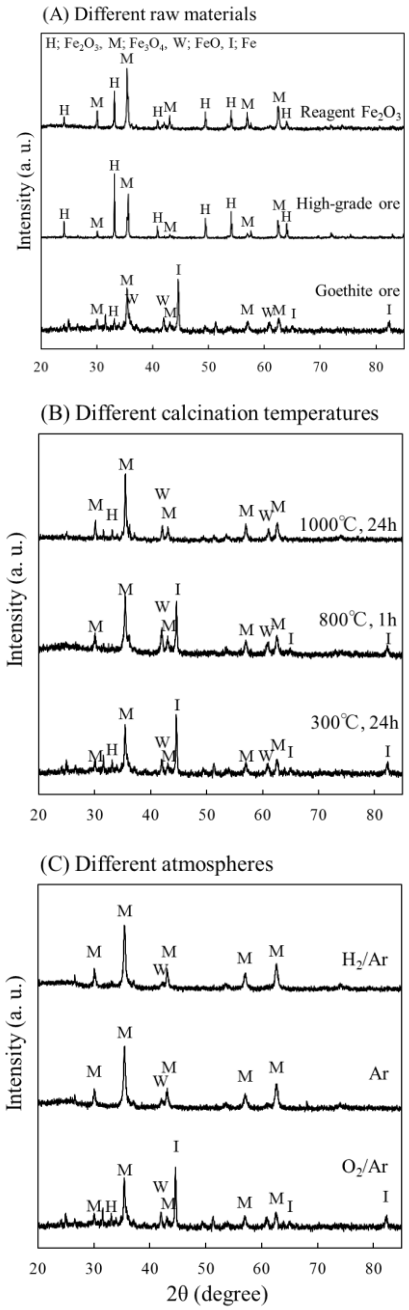

Figure 4-10. XRD patterns of the products from the combustion synthesis experiments. (A) Different raw materials: goethite ore, high-grade ore, and Fe_2O_3 reagent; (B) Different goethite ore calcination temperatures: 300, 800, and 1000 °C; and (C) Different atmospheres: 25 vol%O_2/Ar, Ar, and 20 vol%H_2/Ar were flowed to the carbon-infiltrated goethite ore.

The effect of the nanopores was also investigated by changing the pore structure of the goethite ore using different calcination conditions (i.e., 300 °C for 24 h, 800 °C for 1 h, and 1000 °C for 24 h). As seen in Figure 4-7, different types of pores were obtained after calcination under these conditions. The reduction in the CS experiments proceeded to metallic iron only in the goethite ores pre-calcined at lower temperatures (300 °C and 800 °C, Figure 4-10B). As stated, this can also be understood in terms of the effect of nano-contacts between the goethite ore and carbon. Nanopores in the goethite ore were maintained only when the pre-calcination temperature was below 800 °C; carbon can be easily deposited in such nanopores, resulting in effective contact with the ore.

In addition, the effect of the atmosphere type was also investigated. Carbon-infiltrated goethite ores prepared from the goethite ore viz. calcination at 300 °C for 24 h were used for this purpose. The ores were heated at the same heating rate (of 20 °C s^{-1}) to 900 °C under oxygen (25 vol% O_2/Ar), argon (100 vol% Ar), and hydrogen (20 vol% H_2/Ar) atmospheres. The temperature was maintained for 10 s after reaching 900 °C, after which time the O_2 and H_2 gas flows were stopped. Surprisingly, reduction of the goethite ore proceeded more fully under the oxygen atmosphere (Figure 4-10C). In contrast, reduction proceeded only to Fe_3O_4 and partially to FeO under the argon and hydrogen atmospheres.

There was no difference in the reduction of the carbon-infiltrated goethite ore after the CS experiments under argon and hydrogen atmospheres. According to a previous report, hydrogen reduction of Fe_2O_3 to Fe_3O_4 occurs at 150 °C and the

reduction of Fe_3O_4 to Fe begins at 400 °C [32]. The carbon-infiltrated goethite ores examined in this study were heated to 900 °C and maintained at this temperature during the CS experiments. Although it was possible to reduce the goethite ore at 900 °C under a hydrogen atmosphere, the previously observed effect of hydrogen on the reduction of the goethite ore was not observed at all. This difference is attributed to the formation of a thick, dense carbon layer on the goethite ore surface (Figure 4-9C), which prevented H_2 gas from contacting the goethite ore and reducing it.

Clearly, the highest degree of reduction must occur following carbon combustion at the ore surface. Figure 4-11 shows the temperature and temperature derivative of time during the CS experiments in oxygen, argon, and hydrogen atmospheres.

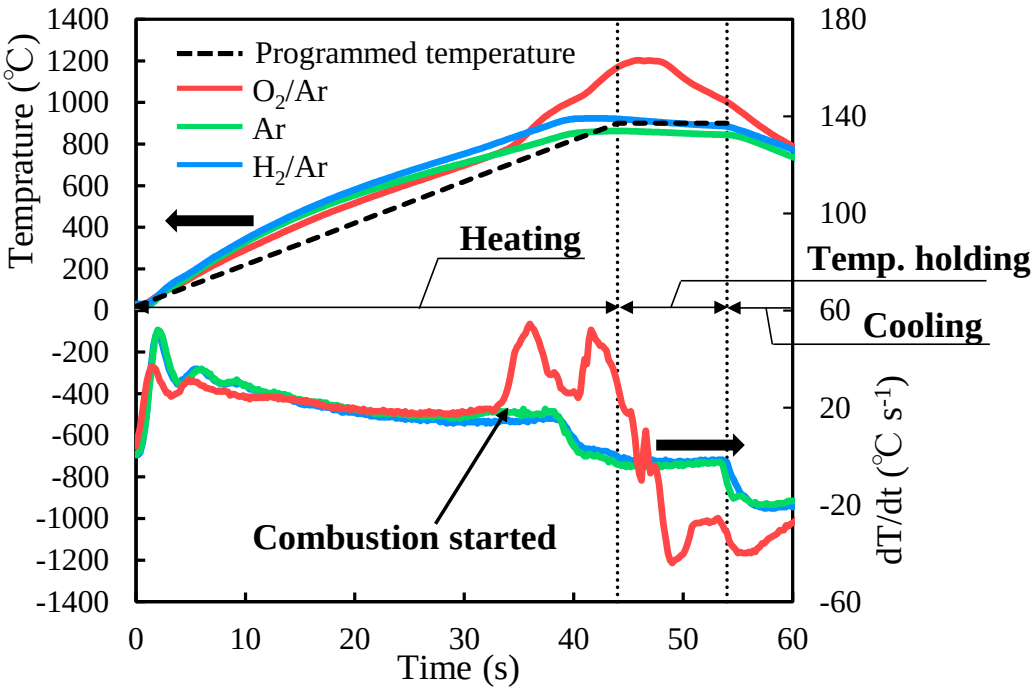

Figure 4-11 Temperature change and temperature derivative of time during the combustion synthesis experiments flowing 25 vol% O_2/Ar, 25 vol% Ar, and 20 vol% H_2/Ar at 900 °C with a programed temperature (black dotted line).

In the case of the argon and hydrogen atmospheres, the temperature was almost identical with the programmed temperature (black dotted line in Figure 4-11). However, the temperature suddenly increased in the oxygen atmosphere, reaching a maximum value of 1200 °C even though the temperature was set to 900 °C. This result demonstrates that carbon combustion occurred at the ore surface and that higher temperatures were obtained only in an oxygen atmosphere. Further, the results suggest that heat generated from the exothermic combustion reaction

transferred to the goethite ore, promoting reduction reactions inside it.

Figure 4-12A shows the gas composition (i.e., O_2, CO, CO_2, H_2, H_2O, and CH_4) of the outflow gases during the CS experiments under an oxygen atmosphere. An increase in the amounts of CO, CO_2, and CH_4 and a decrease in the amount of O_2 were observed. The increase in CO_2 and the decrease in O_2 occurred simultaneously, indicating that O_2 consumption was caused by the combustion of carbon ($C + O_2 \rightarrow CO_2$) at the surface of the carbon-infiltrated goethite ore. After several seconds from the onset of combustion, CO gas was generated, implying that it was produced by the direct reduction reaction between iron oxide and carbon ($FeO_x + C \rightarrow FeO_{x-1} + CO$). The formation of CH_4 may be related to the decomposition of hydrocarbons. Elemental analysis revealed that the carbon deposited in the goethite ore was not pure C; the goethite ore contained 24.4 and 0.64 mass% of C and H, respectively. Some of the carbon was present as hydrocarbons and decomposed to C, CH_4, and other gases at high temperature. In order to verify the reduction mechanism, the carbon-infiltrated goethite ore, which was pre-calcined at 300 °C for 24 h, was heated in an Ar atmosphere at a heating rate of 20 °C min^{-1} until 1000 °C was reached and held at this temperature for 10 s. The composition of CO and CO_2 gases was monitored during the experiment, as shown in Figure 4-12B. As seen, the amount of CO was much higher than that of CO_2, and the CO ratio in CO and CO_2 (i.e., $CO/(CO + CO_2)$) was ~0.85 on average.

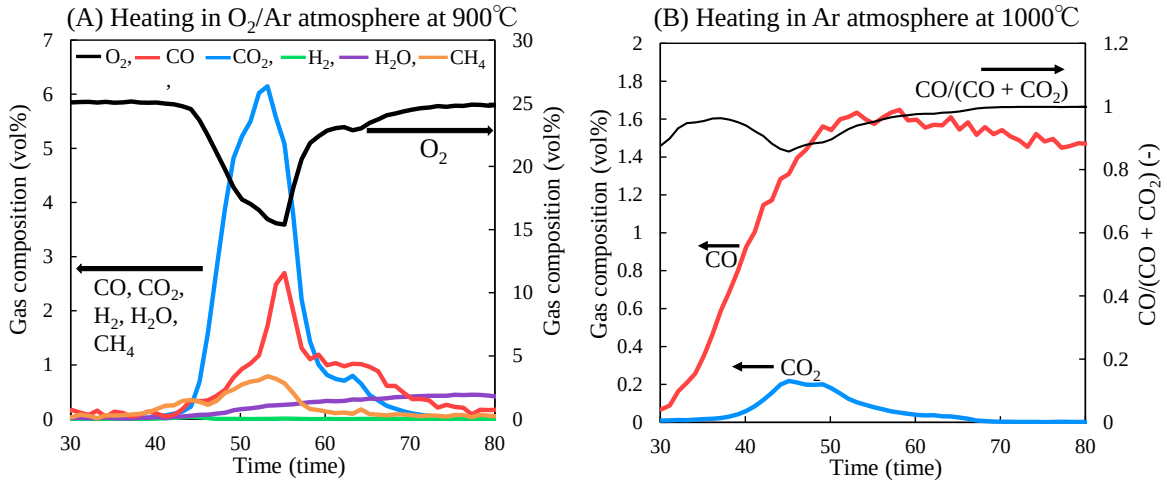

Figure 4-12 Gas compositions of the output gases during combustion synthesis experiments flowing 1 L min^{-1} of 25 vol% O_2/Ar at 900 °C and (B) CO/(CO + CO_2) during heating with Ar flowing at 1000 °C.

The cross-sectional area of the goethite ore after the CS experiments in an oxygen atmosphere was observed using SEM-EDS and light microscopy (Figure 4-13). As seen, the thick carbon layer on the goethite ore surface shown in Figure 2C disappeared due to carbon combustion. Detailed observation near the goethite ore surface revealed that red Fe_2O_3 was formed; re-oxidation partially occurred where the carbon layer completely disappeared. The ore surface without the carbon layer easily contacted oxygen, resulting in a fast oxidation. Clearly, a process to inhibit re-oxidation is essential for carbon combustion synthesis ironmaking.

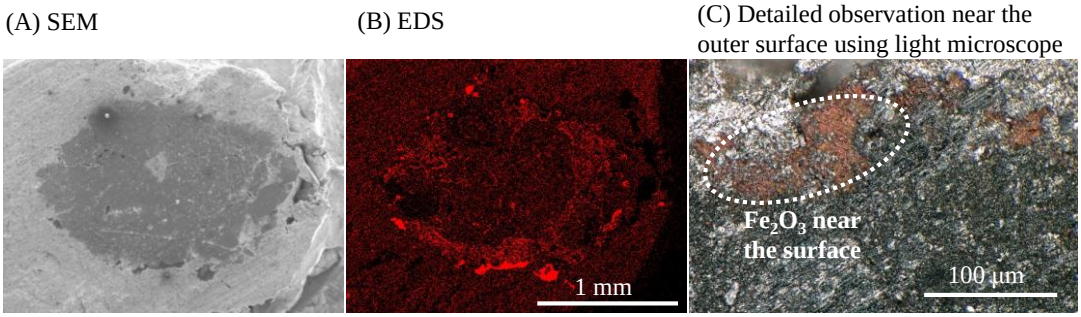

Figure 4-13 Cross-sectional observation of the goethite ore after CS experiments flowing 1 L min^{-1} of 25 vol% O_2/Ar at 900 °C.

The effects of holding temperature of the CS experiments were investigated. Figure 4-14 shows the XRD patterns of the goethite ore after CS experiments. The carbon-infiltrated goethite ore was rapidly heated until 700, 800, 850, and 900℃ flowing 1 L min^{-1} of 25 vol%O_2/Ar at a heating rate of 20℃ s^{-1} and was maintained at those temperatures for 10 s. The holding temperature of 800℃ showed the highest reduction degree; stronger oxide peaks were observed at another temperatures. Figure 4-15 shows the temperature changes measured by a thermocouple placed just above the carbon infiltrated goethite ore during CS experiments. The red dotted lines in the figure mean the holding temperatures of each experiment. The measured temperatures exceeded the holding ones at all temperatures, implying carbon combustion at the surface of the goethite ore successfully occurred in all samples. When the holding temperature was 900℃, carbon combustion started before it reached the holding temperature and finished

at the beginning of the temperature holding (Figure 4-11). This meant almost of all the carbon generated on the goethite ore disappeared during temperature holding. After the death of the surface carbon, flowing O_2 could contact with the goethite ore, resulting in oxidation of goethite ore. When the holding temperature was 700℃, carbon combustion started after it reached the holding temperature. That was why only small part of the surface carbon combusted during the experiments and the goethite ore was kept at higher temperature only for short time, resulting in lower reduction degree.

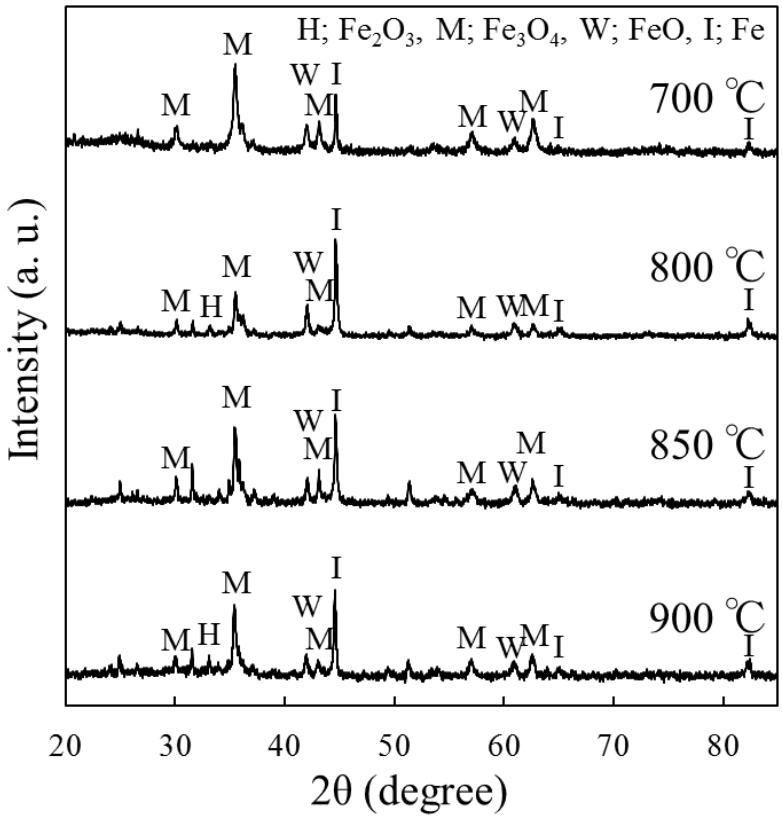

Figure 4-14 XRD patterns of the goethite ore after the CS experiments flowing 1 L min^{-1} of 25 vol%O_2/Ar at 700, 800, 850, and 900℃.

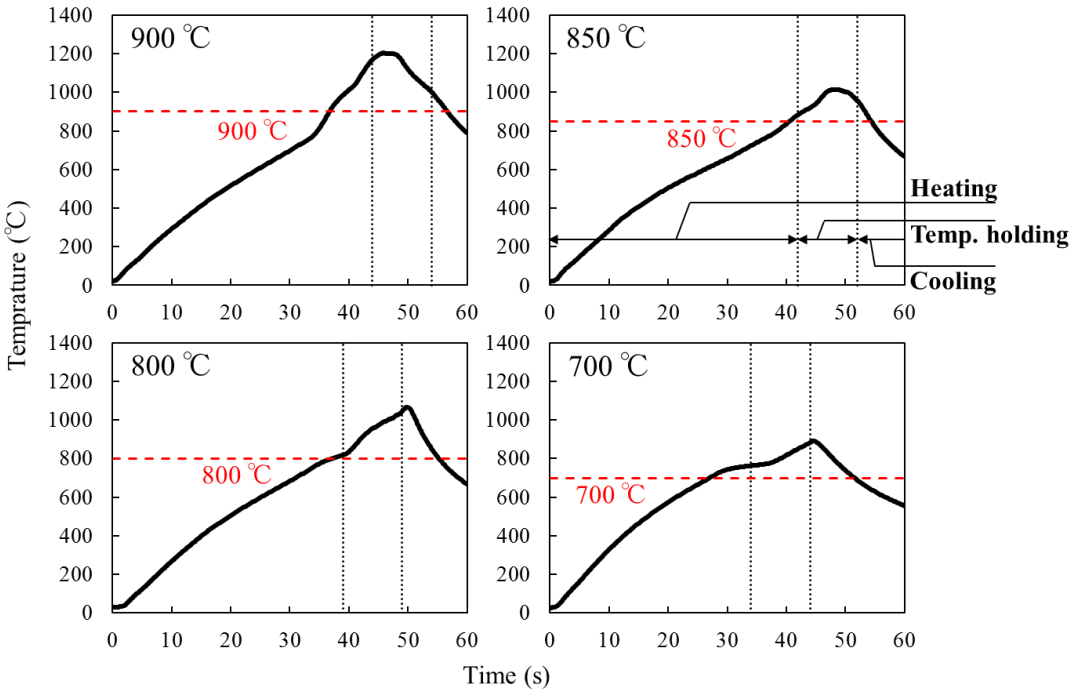

Figure 4-15 Temperature change during CS experiments flowing 1 L min^{-1} of 25 vol%O_2/Ar at 700, 800, 850, and 900℃.

The effects of oxygen concentration in the flowing gases of the CS experiments were investigated. Figure 4-16 shows the XRD patterns of the goethite ore after CS experiments. The carbon-infiltrated goethite ore was rapidly heated up to 900℃ flowing 1 L min^{-1} of 15, 20, 25, 50 and 100 vol%O_2/Ar at a heating rate of 20℃ s^{-1} and was maintained at those temperatures for 10 s. When higher concentration of oxygen gas of over 50% was used, reduction of the goethite ore proceeded only to Fe_3O_4. Lower concentration of oxygen (15-25%) could reduce the goethite ore to metallic iron.

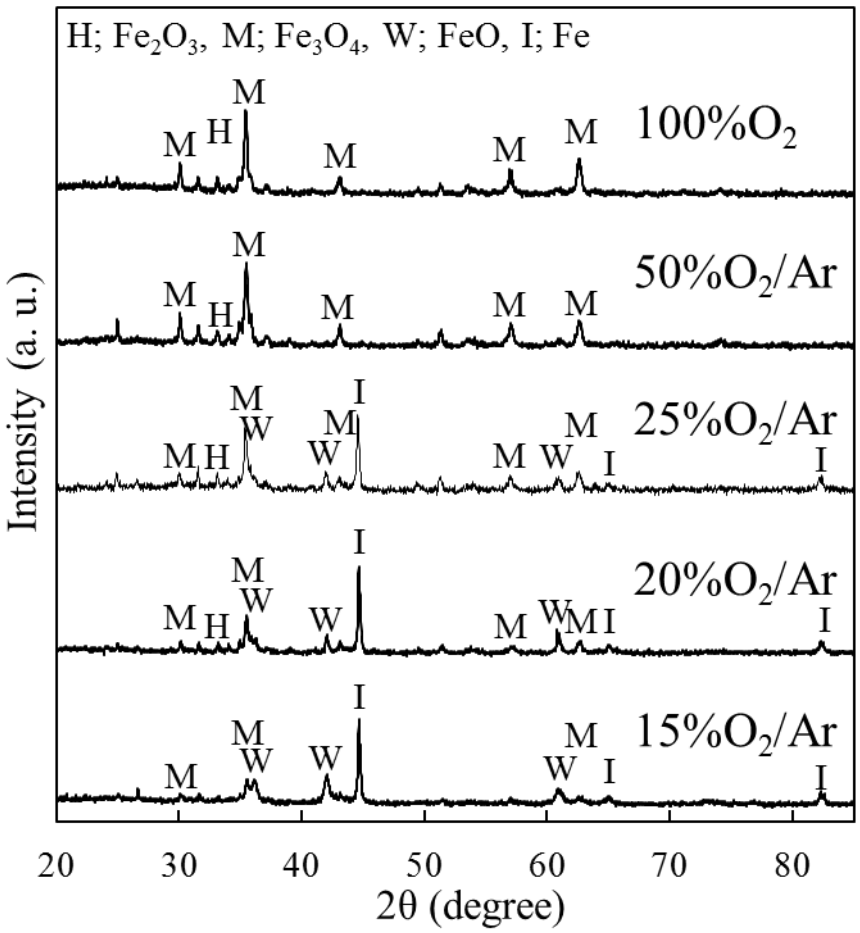

Figure 4-16 XRD patterns of the goethite ore after the CS experiments flowing 1 L min^{-1} of 15, 20, 25, 50, and 100 vol% O_2/Ar at 900 °C.

4-4. Summary

In this study, the probability of the carbon combustion synthesis ironmaking method was investigated by adiabatic flame temperature calculations under some assumptions using a numerical software. 28.9, 27.5, and 23.5wt% of carbon is needed for Fe_2O_3, Fe_3O_4, and FeO when the adiabatic flame temperature was 1800K. The adiabatic flame temperature increased with larger amount of carbon and lower amount of oxygen in iron oxide. Slag components in goethite ore, reactive amorphous carbon, and pre-heating can reduce the amount of essential carbon. The amount of essential carbon can be decreased until 20.5−25.0mass% for the actual carbon infiltrated goethite ore.

Carbon-infiltrated iron ores were prepared from a coal-tar solution and select calcined iron sources (i.e., goethite (FeOOH) ore, high-grade hematite ore, and Fe_2O_3 reagent grain). A several hundred-micrometer thick carbon layer was deposited on the surface of all iron sources. Because the tar solution successfully penetrated into its nanopores, only goethite ore possessed a significant amount of carbon in its interior nanopores. The carbon-infiltrated ores were heated rapidly in an oxygen atmosphere in the combustion synthesis experiments. Carbon combustion occurred at the ore surface, with the ore temperature increasing suddenly during the experiments. Fast reduction to metallic iron was observed only in the carbon-infiltrated goethite ore, regardless of the oxygen atmosphere. Close contact between the goethite ore and the carbon in its interior via the nanopores facilitated the fast reduction. The apparent reduction reaction of the goethite ore is

akin to a direct reduction reaction ($FeO_x + C \rightarrow FeO_{x-1} + CO$).

REFERENCES

[1] Y. Hata, H. Purwanto, S. Hosokai, J. Hayashi, Y. Kashiwaya, and T.Akiyama, Energy & Fuels, 23(2), (2009), pp.1128-1131.

[2] A. N. Rozhan, R. B. Cahyono, N. Yasuda, T. Nomura, S. Hosokai, H. Purwanto, T. Akiyama, Energy and Fuels, 26 (2012), pp.7340-7346.

[3] R. B. Cahyono, A. N. Rozhan, N. Yasuda, T. Nomura, S. Hosokai, Y. Kashiwaya, T. Akiyama, Fuel Processing Technology 113, (2013), pp.84-89.

[4] R. B. Cahyono, A. N. Rozhan, N. Yasuda, T. Nomura, H. Purwanto, T. Akiyama, Energy Fuels 27 (2013), pp 2687–2692.

[5] R.B. Cahyono, N. Yasuda, T. Nomura, T. Akiyama, Fuel Processing Technology 119 (2014), pp. 272-277

[6] A. Kurniawan, K. Abe, T. Nomura, and T. Akiyama, Energy Fuels, in press.

[7] R. B. Cahyono, G. Saito, N. Yasuda, T. Nomura, and T. Akiyama, Energy Fuels, 2014, 28 (3), pp. 2129–2134

[8] S. Hosokai, K. Matsui, N. Okinaka, K. Ohno, M. Shimizu, and T. Akiyama, Energy Fuels, 26 (2012), pp. 7274–7279.

[9] I. Saita, L. Li, K. Saito, T. Akiyama, Journal of Alloys and Compounds 356-357 (2003).

[10] S. K. Dolukhanyan, Journal of Alloys and Compounds 253-254 (1997).

[11] Y. Kitamura, N. Okinaka, T. Shibayama, O. O. P. Mahaney, D. Kusano, B. Ohtani, T. Akiyama; Powder Technology **176** (2007).

[12] H. Ishikawa, T. Akiyama; Journal of Alloys and Compounds **454** (2008).

[13] A. Kikuchi, D. Tran, S. Lin, N. Okinaka, T. Akiyama; Applied Physics Express **5**, 4 (2012).

[14] J. Niu, S. Suzuki, X. Yi, T. Akiyama; Ceramics International **41** (2015).

[15] S. Suzuki, X. Yi, J. Niu, T. Akiyama; Journal of the Society of Powder Technology, Japan **53** (2016).

[16] K. Abe, A. Kikuchi, N. Okinaka, T. Akiyama; Journal of Alloys and Compounds **611** (2014).

[17] N. Yasuda, R. Wakabayashi, S. Sasaki, N. Okinaka, T. Akiyama; International Journal of Hydrogen Energy 34 (2009).

[18] T. Tsuchiya, N. Yasuda, S. Sasaki, N. Okinaka, T. Akiyama; International Journal of Hydrogen Energy 38 (2013).

[19] M. Deguchi, N. Yasuda, C. Zhu, N. Okinaka, T. Akiyama; Journal of Alloys and Compounds 622 (2015).

[20] J. J. Moore, H. J. Feng; Progress in Materials Science **39** (1995).

[21] Mochizuki, Y.; Tsuboushi, N.; Akiyama, T. *Fuel Process. Technol.* **2015**, *138*, 704–713.

[22] Mochizuki, Y.; Nishio, M.; Tsuboushi, N.; Akiyama, T. *Fuel Process. Technol.* **2016**, *142*, 287–295.

[23] Mochizuki, Y.; Nishio, M.; Ma, J.; Tsuboushi, N.; Akiyama, T. *Energy Fuels* **2016**, *30*, 6233–6239.

[24] Landolt-Boinstein: Thermodynamic Properties of Inorganic Material, Scientific Group Thermodata Europe (SGTE), Springer-Verlag, Berlin-Heidelberg, 1999.

[25] Knacke O., Kubaschewski O., Hesselman K., Thermochemical properties of inorganic substances, 2nd ed., Springer-Verlag, Berlin, 1991.

[26] Bard A. J., Parsons R., Jordan J., Standard potentials in aqueous solution, Marcel Dekker Inc., New York, 1985.

[27] JANAF Thermochemical Tables, 3rd ed., M.W. Chase, et. al., eds., J. of Phys. and Chem. Ref. Data, Vol.14, Suppl.1, 1985.

[28] Glushko Thermocenter of the Russian Academy of Sciences, IVTAN Association, Izhorskaya 13/19, 127412 Moscow, Russia (1994).

[29] Saito, G.; Nomura, T.; Sakaguchi, N.; Akiyama, T. *ISIJ Int.* **2016**, *56*, 1598–1605.

[30] Barrett, E.P.; Joyner, L.G.; Halenda, P.P. *J. Am. Chem. Soc.* **1951**, *73*, 373–380.

[31] Naono, H.; Nakai, K.; Sueyoshi, T.; Yagi, H. *J. Colloid and Interface Sci.* **1987**, *120*, 439–450.

[32] Jozwiak, W.K.; Kaczmarek, E.; Maniecki, T.P.; Ignaczak, W.; Maniukiewicz, W. *Appl. Catal. A* **2007**, *326*, 17–21.

Chapter 5

General Conclusion

The ironmaking industry is facing three significant problems about resource (degraded high grade iron ore), energy (a lot of unutilized high-temperature waste heat), and environment (CO_2 emission). Goethite (FeOOH) ore, which has relative low iron contents because of combined water, has been utilized in the industry as an alternative raw material of high-grade iron ore. Goethite ore in the actual ironmaking process is heated at high temperature in the sintering process before it is put into blast furnace. However, the goethite ore becomes nanoporous after mild calcination at around 300℃. In this study, processes to solve the problems of the ironmaking industry using this nanoporous goethite-based ore were proposed and examined; (1) Ni-containing goethite ore utilization as a catalyst for the dry reforming of methane and (2) coke free fast ironmaking method using carbon infiltrated goethite ore.

Chapter 1 provided the general introduction of this thesis.

Chapter 2 described Ni-containing goethite ore as a catalyst for the dry reforming of methane ($CH_4 + CO_2 \rightarrow 2H_2 + 2CO$). Ni-based catalysts are generally utilized in this reaction, however, the production processes are very complex and the conventional catalysts are expensive to produce. In this study, cheap goethite ore catalyst was focused on and the catalytic performance of the goethite ore was

observed. Goethite based ores which have different amounts of Ni were prepared. The ores were compared their catalytic performance by catalytic tests at several conditions. The ore containing larger amount of Ni showed higher catalytic performance, meaning the Ni in the ore effectively worked as a catalyst in the dry reforming reaction. The catalytic performance of the Ni-containing goethite ore was compared with Ni-supported goethite ore by wet impregnation method. They had almost same Ni amount, however, the Ni-containing goethite ore showed much higher catalytic performance. That was because the different sizes of Ni particle in the ores. TEM-EDS observation revealed that Ni in the goethite ore was homogeneously distributed and the supported Ni had larger size around 20 nm.

Chapter 3 described the effects of hydrogen reduction on the catalytic performance of the Ni-containing goethite ore in the dry reforming reaction. The main phase of the goethite ore after mild calcination is Fe_2O_3 and the Fe_2O_3 can be easily reduced in hydrogen or carbon monoxide atmosphere. This caused the different reduction degrees of the goethite ore during the catalytic tests. In this study, pre-reduction and hydrogen flowing during catalytic tests were tried to control the reduction degrees of the goethite ore and the effects of reduction were observed. The phase of iron in the goethite ore changed to oxides (Fe_3O_4 and FeO) and metals (Fe and Fe-Ni) during the catalytic tests. When the iron mainly existed as oxides, the catalytic performance of the FeO was better than that of Fe_3O_4. Fe and Fe-Ni showed much greater catalytic performance than the oxides. The catalytic performance which was normalized by the Ni content of the Ni supported Al_2O_3 catalyst was better than that of the Ni-containing goethite ore catalyst due to the

effect of catalyst support, however, the ore catalyst was more stable during catalytic use and much cheaper than the Ni/Al_2O_3.

Chapter 4 described proposal of a fast ironmaking method using carbon infiltrated goethite ore in an oxygen atmosphere, "combustion synthesis ironmaking", theoretical calculation of the possible conditions of the proposed method, and experimental investigation of the method. The combustion synthesis reaction automatically proceeds by self-propagation of the combustion wave after ignition. The self-propagation occurs experientially at the adiabatic temperature over 1800 K. In this study, adiabatic temperature calculations were taken place for carbon infiltrated iron oxides. Different carbon contents and different compositions of the starting iron oxide were tried to check up the possible conditions of the combustion synthesis ironmaking method. Carbon infiltrated iron ores were produced and combustion synthesis experiments were taken place using the ores. Coal-tar solution and some iron sources (goethite ore, high-grade ore, and reagent Fe_2O_3 grain) were prepared to make the carbon infiltrated iron ores. Thick carbon layer of several hundred micrometers was deposited on the surface of the iron sources. The tar solution penetrated into its nanopores of the calcined goethite ore, the goethite ore had a large amount of carbon in its interior nanopores. The carbon infiltrated iron ores were rapidly heated in an oxygen atmosphere in the combustion synthesis experiments. During the experiments, carbon combustion occurred at surface of the iron ores, with sudden increase of the ore temperature. Fast reduction to metallic iron was observed only in the carbon infiltrated goethite ore. Close contact between the goethite ore and the carbon in its interior via the nanopores

facilitated the fast reduction. The apparent reduction reaction of the goethite ore is akin to a direct reduction reaction ($FeO_x + C \rightarrow FeO_{x-1} + CO$).

APPENDIX

Publications

1. ***Keisuke Abe***, Asami Kikuchi, Noriyuki Okinaka, Tomohiro Akiyama, "Single Thermite-type combustion synthesis of Fe_2VAl for thermoelectric applications from Fe, V_2O_5, and Al powders", Journal of Alloys and Compounds, 611 (2014), 319-323.
2. ***Keisuke Abe***, Genki Saito, Takahiro Nomura, Tomohiro Akiyama, "Limonitic Laterite Ore as a Catalyst for the Dry Reforming of Methane", Energy and Fuels **30** (2016), 8457-8462.
3. ***Keisuke Abe***, Ade Kurniawan, Takahiro Nomura, Tomohiro Akiyama, "Effects of Reduction on the Catalytic Performance of Limonite Ore for Dry Reforming Reaction", Journal of Energy Chemistry, in press.
4. Ade Kurniawan, ***Keisuke Abe***, Takahiro Nomura, Tomohiro Akiyama, "Integrated Pyrolysis-Tar Decomposition over Low-Grade Iron Ore for Ironmaking Applications: Effects of Coal-Biomass Fuel Blending", Energy and Fuels, in press.

Presentations (Domestic)

1. ***Keisuke Abe***, Asami, Kikuchi, Noriyuki Okinaka, Tomohiro Akiyama, "Single Thermite-type Combustion Synthesis of Fe_2VAl", The Mining and Materials Processing Institute of Japan, Hokkaido University, 3-5 September, 2013

2. ***Keisuke Abe***, Asami, Kikuchi, Noriyuki Okinaka, Tomohiro Akiyama, "Single Thermite-type Combustion Synthesis of Fe_2VAl for Thermoelectrics", 166th The Iron and Steel Institute of Japan, Kanazawa University, 17-19 September, 2013
3. ***Keisuke Abe***, Asami, Kikuchi, Noriyuki Okinaka, Tomohiro Akiyama, "Effects of ball-milling time on the Thermal Conductivity of Combustion Synthesized and Spark Plasma Sintered Fe_2VAl", Summer Session of The Japan Institute of Metals and Materials and The Iron and Steel Institute of Japan, Hokkaido University, 28 July, 2014
4. ***Keisuke Abe***, Asami, Kikuchi, Noriyuki Okinaka, Tomohiro Akiyama, "Synthesis of Heusler Alloy Fe_2VAl by Combustion Synthesis and Spark Plasma Sintering", 11th Annual Meeting of the Thermoelectrics Society of Japan, National Institute for Materials Science, Tsukuba, 29-30 September, 2014
5. ***Keisuke Abe***, Rochim Bakti Cahyono, Takahiro Nomura, Tomohiro Akiyama, "Chemical Vapor Infiltration (CVI) Ironmaking Process Using Pisolite Ore and Some Carbon Sources", 1st Ironmaking 54 Committee of Japan Society for the Promotion of Science, Hokkaido University, 2-3 July, 2015
6. ***Keisuke Abe***, Takahiro Nomura, Tomohiro Akiyama, "Catalytic properties of Ni-containing porous iron ore", 47th Autumn Meeting of The Society of Chemical Engineers Japan, Hokkaido University, 9-11 September, 2015
7. ***Keisuke Abe***, Genki Saito, Takahiro Nomura, Tomohiro Akiyama, "Catalytic performance of Ni-containing porous iron ore in the CO_2 reforming of methane",

Winter Session of The Japan Institute of Metals and Materials and The Iron and Steel Institute of Japan, Hokkaido University, 17-18 December, 2015

8. ***Keisuke Abe***, Genki Saito, Takahiro Nomura, Tomohiro Akiyama, "Catalytic application of Ni-contained low grade iron ore", 171st The Iron and Steel Institute of Japan, Tokyo University of Science, 23-25 March, 2016
9. ***Keisuke Abe***, Ade Kurniawan, Takahiro Nomura, Tomohiro Akiyama, "Catalytic performance of laterite ore after hydrogen reduction", 172nd The Iron and Steel Institute of Japan, Osaka University, 21-23 September, 2016
10. ***Keisuke Abe***, Ade Kurniawan, Kouichi Ohashi, Takahiro Nomura, Tomohiro Akiyama, "Feasibility of Ironmaking by Carbon Combustion Synthesis", 174th The Iron and Steel Institute of Japan, Hokkaido University, 7-9 September, 2017

Presentations (International)

1. ***Keisuke Abe***, Asami Kikuchi, Noriyuki Okinaka, Tomohiro Akiyama, "Thermite-Type Combustion Synthesis of Heusler-Alloy Fe_2VAl for Thermoelectric Materials", 3rd International Doctoral Student Symposium on Material Science (IDSS-3), Hokkaido University, 25-28 February, 2015
2. ***Keisuke Abe***, Genki Saito, Takahiro Nomura, Tomohiro Akiyama, "Catalytic application of Ni-containing low grade iron ore", The 14th Symposium between University of Science and Technology of Beijing & Hokkaido Univeristy, University of Science and Technology of Beijing, 6-9 March, 2016

3. ***Keisuke Abe***, Ade Kurniawan, Takahiro Nomura, Tomohiro Akiyama, "Hydrogen Generation via Some Catalytic Reactions over Limonite Ore", 1st International Conference on Energy and Materials Efficiency and CO_2 Reduction in the Steel Industry (EMECR2017), Kobe International Conference Center, 11-13 October, 2017

Awards

1. Tomohiro Akiyama, Asami Kikuchi, ***Keisuke Abe***, Noriyuki Okinaka, "Best Paper Prize of The 7th International Exergy, Energy and Environment Symposium", 30 April, 2015.
2. ***Keisuke Abe***, Rochim Bakti Cahyono, Takahiro Nomura, Tomohiro Akiyama, "Encouragement Prize of 1st Ironmaking 54 Committee of Japan Society for the Promotion of Science", 3 July, 2015.
3. ***Keisuke Abe***, Genki Saito, Takahiro Nomura, Tomohiro Akiyama, "Encouragement Prize of Winter Session of The Japan Institute of Metals and Materials and The Iron and Steel Institute of Japan", 18 December, 2015.
4. ***Keisuke Abe***, Genki Saito, Takahiro Nomura, Tomohiro Akiyama, "Effort Award of 171st The Iron and Steel Institute of Japan", 24 March, 2016.
5. ***Keisuke Abe***, Ade Kurniawan, Kouichi Ohashi, Takahiro Nomura, Tomohiro Akiyama, "Effort Award of 174th The Iron and Steel Institute of Japan", 8 September, 2017.

Acknowledgement

First of all, I am deeply grateful to the supervisor, Prof. Tomohiro Akiyama, professor of the Center for Advanced Research of Energy and Materials, Hokkaido University. Without his practical advice and positive encouragements throughout this research, this dissertation would not have been possible.

I also would like to extend my gratitude to each committee: Prof. Shigeharu Ukai, Prof. Seiichi Watanabe, Associate Prof. Yoshiaki Kashiwaya, and Associate Prof. Takahiro Nomura, who reviewed this dissertation, for their valuable comments and helpful advice.

I am grateful to my co-researchers: Dr. Genki Saito, Mr. Ade Kurniawan, Mr. Kouichi Ohashi, and Mr. Masafumi Sanada. They always gives me insightful suggestions and comments. Especially, Dr. Genki Saito helps me to conduct TEM experiments for nanostructure observation. I also want to thank all the members in the Laboratory of Energy Media for their kind help and encouragement.

I would also like to express my gratitude to my family for their moral support and warm encouragement.

This research was partly supported by a Grant-in-Aid for Japan Society of Promotion of Science (JSPS) Fellows.